THE EFFECT OF NANOPARTICLES ON THE THERMAL TRANSITIONS OF HYDRATED LAYER-BY-LAYER ASSEMBLIES

A Thesis

by

JOSEPH TIMOTHY PUHR

Submitted to the Office of Graduate and Professional Studies of
Texas A&M University
in partial fulfillment of the requirements for the degree of

MASTER OF SCIENCE

Chair of Committee,	Jodie L. Lutkenhaus
Committee Members,	Jamie C. Grunlan
	Michael J. McShane
Head of Department,	Ibrahim Karaman

May 2014

Major Subject: Material Science & Engineering

ABSTRACT

Nanoparticles can have a profound effect on a polymer's glass transition temperature (T_g). Many layer-by-layer (LbL) assemblies contain nanoparticles for added functionality, but the resulting effect of nanoparticles on an LbL film's properties is not known. Previously, we have shown that a nanoparticle-free LbL film containing strong polyelectrolytes, poly(diallyldimethylammonium chloride)/poly(styrene sulfonate) (PDAC/PSS), exhibited a thermal transition somewhat akin to a glass transition using quartz crystal microblance with dissipation (QCM-D) and modulated differential scanning calorimetry (MDSC). In the work presented here, layers of negatively charged nanoparticles of either spherical or platelet morphology have been inserted at varying locations throughout PDAC/PSS LbL films. QCM-D and MDSC were used to determine the effect that these nanoparticles have on the previously measured thermal transitions as a function of placement within the film and particle shape. Using QCM-D we observed clear, reproducible T_g's in all LAP film configurations and in one particular SiO_2 configuration. All observed T_g's, regardless of nanoparticle morphology, were elevated with respect to those found in neat PDAC/PSS films. Additionally, there was little difference noted between the transition values for the two particular morphologies. It was discovered that the highest glass transition temperatures were observed for film configurations where the nanoparticles were added during the middle bilayer. We attributed this phenomenon to the increased available nanoparticle surface area with which nearby polymer chains could form bonds. Unfortunately the extremely weak and

broad thermal transitions observed with MDSC proved to be inconclusive in either supporting or refuting these observations made via QCM-D.

DEDICATION

I would like to dedicate this thesis work to my parents. Their love and support was so important in keeping me motivated throughout the course of graduate school.

ACKNOWLEDGEMENTS

I would like to thank my committee chair, Dr. Lutkenhaus, and my committee members, Dr. Grunlan and Dr. McShane, for their guidance and support throughout the course of this research.

Thanks also go to my friends and colleagues and the department faculty and staff for making my time at Texas A&M University a great experience.

Finally, thanks to my family for their unwavering love and encouragement. I am so incredibly blessed to have them in my life.

NOMENCLATURE

Δf	Frequency
ΔD	Dissipation
MDSC	Modulated Differential Scanning Calorimetry
LbL	Layer-by-Layer
PDAC	Poly(diallyldimethylammonium chloride)
PEI	Poly(ethylene imine)
PSS	Poly(styrene sulfonate)
QCM-D	Quartz Crystal Microbalance with Dissipation
T_g	Glass Transition Temperature

TABLE OF CONTENTS

Page

LIST OF FIGURES

Page

LIST OF TABLES

1. AN INTRODUCTION TO LAYER-BY-LAYER (LBL) ASSEMBLY

Layer-by-layer (LbL) assembly, a process by which nanoscale films are made through the alternating adsorption of oppositely charged species, was first demonstrated by Iler et al. in the mid-1960's, but largely forgotten until a publication by Decher *et al.* in the early 1990's [1, 2]. Since then this cost-effective technique has expanded to include a diverse array of materials (polymers, nanoparticles, and certain biomaterials to name a few), and also has been shown to be suitable for a host of applications ranging from optics to drug delivery [3-8]. A major reason why LbL assembly has been so successful is due to the fact that it is possible to produce films of uniform thickness on substrates of all shapes and sizes [1]. In addition, precise control of film properties can be exercised simply by adjusting parameters such as ionic strength, salt type, pH, solvent quality, temperature, and humidity [9-20].

1.1 POLYELECTROLYTES

Prior to truly delving into the methodology behind LbL assembly, it is necessary to first define polyelectrolytes. Polyelectrolytes are charged polymer chains that can be classified as strong or weak. As one may guess based on their names, strong polyelectrolytes have strongly dissociated cationic or anionic repeat units, whereas weak polyelectrolytes are either weak acids or bases. It has become convention in the LbL community to utilize certain "model systems" of polyelectrolytes in order to gain an

understanding of general trends. The two model systems described throughout this introduction are poly(diallyldimethylammonium chloride)/poly(styrene sulfonate) (PDAC/PSS) and poly(allylamine hydrochloride)/poly(acrylic acid) (PAH/PAA), which correspond to strong and weak systems respectively. These polyelectrolytes are depicted in Figure 1 below.

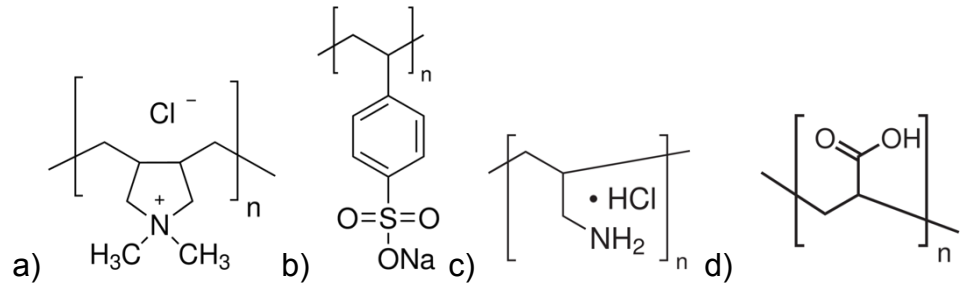

Figure 1. Structures of four model strong and weak polyelectrolytes. a) PDAC - Strong; b) PSS - Strong; c) PAH - Weak; d) PAA - Weak.

1.2 THE ASSEMBLY PROCESS

LbL assembly is a process that can be performed either by hand or by means of a programmable robot. In its most basic form, LbL assembly entails exposing a charged substrate to a polyelectrolyte of an opposite charge. This polyelectrolyte will then adsorb to the substrate surface, resulting in a charge reversal. Charge reversal is the key component to LbL assembly in that it limits adsorption of similarly charged polyelectrolytes to a finite amount. In addition, the charge reversal enables the adsorption of an oppositely charged polyelectrolyte to occur. These two adsorbed

polyelectrolyte layers make up what is known as a bilayer. It is thus a simple matter to build up a multilayer film by repeating the cycle as many times as desired. Important to note is that a rinsing step is typically utilized in between each adsorption step. This rinse serves to remove weakly bonded polyelectrolyte chains that could potentially contaminate other solutions later on during the LbL assembly process. An example of the LbL assembly process involving a generic polyanion and polycation is shown schematically in Figure 2 below [1].

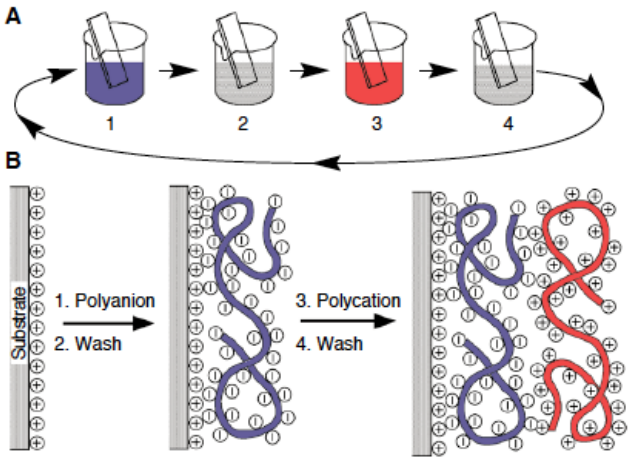

Figure 2. General overview of the LbL assembly process. Part a) depicts assembly on the beaker-scale, while part b) depicts a molecular-scale schematic of LbL assembly involving two polyelectrolytes. From [Decher, G. *Science.* **1997,** *277,* 1232]. Reprinted with permission from AAAS.

1.3 AVAILABLE LBL FABRICATION TECHNIQUES

The LbL assembly procedure depicted in Figure 2 is a dipping method. While dipping is very simple, it is also plagued by long assembly times. A typical single layer

adsorption step requires submersing the substrate into a polyelectrolyte solution for fifteen minutes, while the rinsing step involves dipping in three separate rinse solutions for two, one, and one-minute segments. The roughly forty minute time period required to assemble a bilayer is currently a major hurdle preventing widespread adoption in industry. A much more promising method in terms of industrial applicability is spray LbL assembly. First introduced by Schlenoff *et al.* in 2000, this method has been shown to produce films of nearly similar morphology, uniformity, and chemical composition to that of the dipping method pioneered by Decher, but in only a fraction of the time [21]. A dramatic example of the time saved using this spray method was demonstrated by Nogueria *et al.*, in which optical coatings fabricated via spray LbL assembly were produced 24 times faster than by means of the more conventional dipping method [22].

1.4 COMPOSITION AND CONTROLLABILITY OF POLYELECTROLYTE LBL FILMS

Depending upon whether LbL films are composed of strong or weak polyelectrolytes will determine the parameters one must modify in order to tailor the properties of a film. Strong polyelectrolyte LbL systems, such as PDAC/PSS are most commonly modified through variation of the polymer solution ionic strength [9-13]. On the other hand, for weak polyelectrolyte LbL systems such as PAH/PAA, simple pH adjustments of the assembly solutions are used in order to control both the adsorbed layer thickness and the molecular organization [14, 15].

The ionic strength of a strong polyelectrolyte solution will determine the thickness of the deposited polymer layer; with no salt corresponding to thin layers that grow in a linear fashion, and higher salt concentrations leading to thicker layers that grow exponentially. As the salt ions and water molecules permeate the film, swelling occurs. Interestingly, it has been shown that while polymer adsorption is irreversible, swelling due to the salt ions and water molecules is reversible [12]. This swelling, plus the fact that the salt ions screen the charges along the polyelectrolyte chain, lead to a reduction of segment-segment repulsion. Schlenoff et al. described this salt-screening process, illustrated in Figure 3 below, as extrinsic compensation [12].

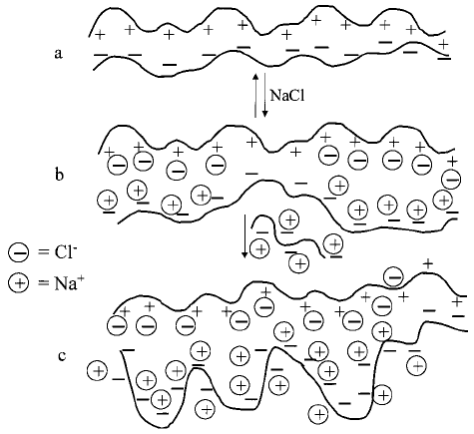

Figure 3. Influence of ionic strength on bonding within LbL assemblies. Part a) corresponds to intrinsic (polyelectrolyte-polyelectrolyte pairing) compensation, part b) corresponds to extrinsic (salt-polyelectrolyte pairing) compensation, and part c) depicts the view of a polyelectrolyte chain approaching the overcompensated film surface. Reprinted (adapted) with permission from (Schlenoff, J. B.; Dubas, S. T. *Macromolecules.* **2001,** *34,* 592.). Copyright (2014) American Chemical Society.

The decreased repulsion allows for additional polymer to adsorb to the film surface since excess charge can now be better distributed throughout the film. Thus in the presence of salt, individual layer thickness will increase as the assembly process progresses. It is worthwhile to note that there is a maximum ionic concentration up to which LbL assemblies can successfully fabricated. In the case of PDAC/PSS films this concentration has been estimated to be roughly 3.5 M NaCl [12]. Beyond this critical concentration the film dissociates since there are not enough polymer-polymer interactions remaining to hold the film together.

The pH adjustments used to tailor the properties of weak polyelectrolyte LbL films directly affect the degree of ionization along the polymer chain [14]. For example, by setting the solution pH to slightly reduce the polyelectrolyte charge density from its fully charged state, large increases in the layer thickness will occur [15]. This is due to the fact that as the charge density drops from the critical level necessary to maintain the adsorbing polymer chain in a flattened conformation, a more loopy conformation results, hence the sizable thickness change [14]. In the case of the PAH/PAA system, both Shiratori *et al.* and Bieker *et al.* were instrumental in identifying four pH ranges that correspond to specific growth behaviors [15, 23]. Figure 4, taken from the study by Shiratori *et al.*, is an effective illustration of the wide range of obtainable PAH/PAA thicknesses [15] found in those four regions.

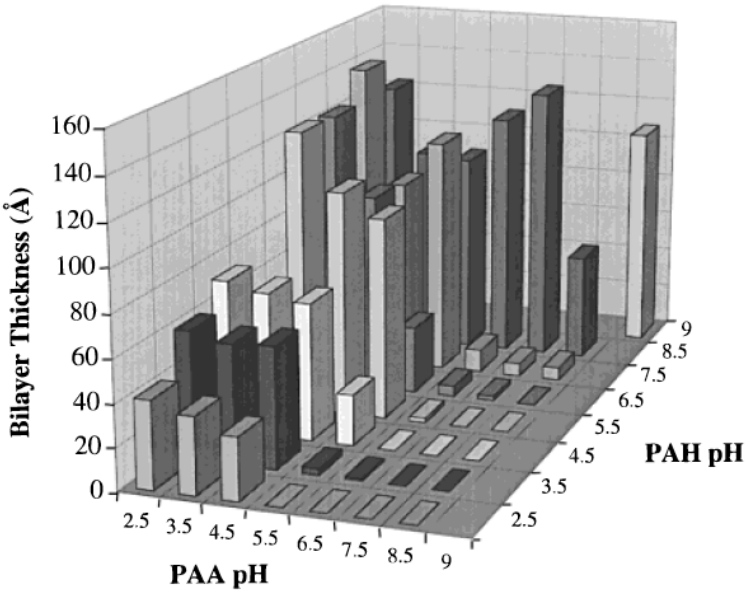

Figure 4. Matrix of thicknesses obtained for PAH/PAA films assembled at various pH values. Reprinted (adapted) with permission from (Shiratori, S. S.; Rubner, M. F. *Macromolecules.* **2000,** *33,* 4213.). Copyright (2014) American Chemical Society.

In the first such pH region (pH 3-4.5) PAA is partially charged, while PAH is completely charged. As a result soft films with large bilayer thicknesses are formed. For the second pH region (4.5-6) both polyelectrolytes are partially charged, and thus thicker and less soft films (relative to those in the 3-4.5 pH range) are produced. In the third pH region (6.5-8) PAH and PAA are both fully charged, and therefore very thin and rigid films are made. The last pH region (pH 8-10) corresponds to PAH being partially charged, while PAA is completely charged. These particular films were found be relatively soft and fairly thick. Additionally, it was found that films formed under the conditions described in the first and third regions grew linearly, while those in the second and fourth regions mainly grew exponentially.

2. THERMAL ANALYSIS OF LBL FILMS

One of the remaining problems to be solved involving LbL films is that of their thermal properties, particularly the glass transition temperature (T_g). Clearly this is an important issue considering that the viability of LbL films in certain applications depends on whether they are glassy or rubbery. Contrary to what one might expect, LbL films are not composed of distinctly stratified layers. Rather it has been shown by multiple research groups that these films are actually quite interpenetrated, with "fuzzy" regions between neighboring layers [1, 24, 25]. Thus when studying the thermal properties of LbL films it is often assumed that one can treat these films as miscible blends.

Over the past few years there have been several noteworthy studies devoted to investigating the thermal properties of LbL films, predominantly with the strong polyelectrolyte system PDAC/PSS. For example Kohler *et al.* performed several experiments on PDAC/PSS capsules in order to better understand their thermal behavior. It was found that capsules terminated with a PSS layer will shrink due to a glassy-viscoelastic transition around 35 °C [26]. On the other hand, capsules terminated with PDAC would swell until rupturing above 55 °C. This phenomenon is commonly called the "odd-even" effect. Mueller *et al.* further corroborated this glass-melt transition for PDAC/PSS capsules by measuring the Young's modulus response to temperature [27]. It was discovered that the modulus decreases from the 100 MPa region to the MPa region at 35 °C. A study by Nazaran *et al.* reported that the lateral mobility observed in

PDAC/PSS LbL films increased by two orders of magnitude while raising the temperature up to 65 °C, indicating that a thermal transition does potentially occur within the film [28]. However, in a paper by Ghostine *et al.*, it was reported that no transition was observed in PDAC/PSS films [29]. In this experiment the diffusion of ferracyanide through PDAC/PSS films with respect to temperature was monitored. Rather than a transition, just a continual increase in chain mobility was observed.

As seen by just that small sampling of prior reports, it is clearly quite difficult to measure the thermal properties of LbL films reliably. One such hurdle is that isolating these films from their substrates in measurable quantities can be extremely tough. Recent developments have made strides toward solving this issue though, in particular the technique to use substrates of low surface energy such as Teflon® [30]. The two images in Figure 5 below depict free-standing films of PDAC/PSS and PAH/PAA respectively:

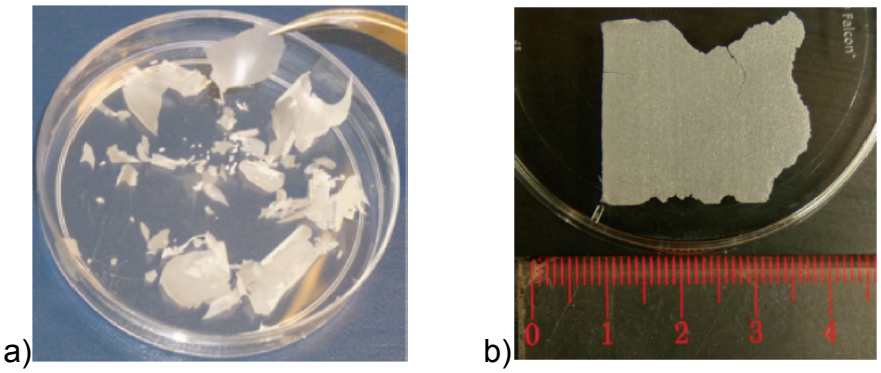

Figure 5. Free-standing LbL films. Part a) depicts the PDAC/PSS system, while part b) depicts the PAH/PAA system. Figure 5a was reprinted (adapted) with permission from (Vidyasagar, A.; Sung, C.; Gamble, R.; Lutkenhaus, J. L. *ACS Nano.* **2012,** *6,* 6174.). Copyright (2014) American Chemical Society. Figure 5b was reprinted (adapted) from {Shao, L.; Lutkenhaus, J. L. *Soft Matter.* **2010,** *6,* 3363.} with permission of The Royal Society of Chemistry.

The use of Teflon® allows for the easy generation of free-standing LbL films that can later be analyzed via conventional thermal analysis methods such as differential scanning calorimetry (DSC). While conventional DSC is generally quite effective for studying thermal transitions, a different variation called modulated DSC (MDSC) is actually better for probing weaker transitions such as those seen in LbL films. Another challenge in studying the thermal properties of LbL films concerns the differences between their dry and hydrated states. MDSC can be utilized to study both states, however sometimes the thermal transitions in hydrated films are too weak for even MDSC to detect consistently. A relatively new technique sensitive enough to study these weaker transitions in hydrated LbL films is quartz crystal microbalance with dissipation (QCM-D). The following subsections seek to provide an in-depth look at both QCM-D and MDSC and their use in studying the thermal properties of both the PDAC/PSS and PAH/PAA LbL systems.

2.1 QUARTZ CRYSTAL MICROBALANCE WITH DISSIPATION (QCM-D)

Quartz crystal microbalance with dissipation (QCM-D) measures changes in both frequency (Δf) and dissipation (ΔD) for films deposited on a quartz crystal. Since quartz is piezoelectric, by applying a voltage across the quartz crystal it is possible to induce an oscillation at a resonant frequency. Therefore any polyelectrolyte added to the surface of the crystal will reduce the frequency of oscillation. As long as the film is rigid, uniformly distributed, and of a smaller mass than the crystal itself, then a linear

relationship between Δf and mass is obeyed. This is known as the Sauerbrey relation [31, 32, 33]:

$$\Delta m = -C\left(\frac{\Delta f}{n}\right) \tag{2.1}$$

where C refers to a sensitivity constant and n is the overtone number of the oscillating frequency (n = 1, 3, 5, 7, 9, 11, 13). However if the film is viscoelastic (i.e. possessing of both viscous and elastic attributes), then complex models such as the Voigt model must be used [34]. The unique aspect of QCM-D is the ability to measure the dissipation of a film. Dissipation is related to film viscoelasticity, and can be determined by removing the applied voltage and observing the decay of the crystal oscillation. Dissipation change, ΔD, is given by [31, 32]:

$$\Delta D = \frac{E_{dissipated}}{2\prod E_{stored}} \tag{2.2}$$

In order to perform thermal analysis using QCM-D, an LbL film assembled on a crystal surface is ramped upwards using a high temperature flow cell. Both Δf and ΔD are monitored throughout the entire process.

2.2 MODULATED DIFFERENTIAL SCANNING CALORIMETRY (MDSC)

Modulated DSC differs from conventional DSC in that rather than just a linear temperature ramp, both superimposed sinusoidal and linear temperature profiles are utilized. Therefore it becomes possible to separate overlapping thermal phenomena. As already mentioned above, it can be especially useful for weak transitions. The total heat flow measured via MDSC (related to the heat flow from a conventional DSC) is the sum

of both the "reversing heat flow" and the "non-reversing heat flow." The former curve contains thermal events that occur quickly, i.e. shorter than the modulation period, and is similar to the sample's heat capacity. Typical thermal events found in this curve are melting and glass transitions. The latter curve corresponds to thermal events that take place over longer time scales, i.e. more slowly than the modulation period. This is similar to kinetic events like cross-linking, volatilization, and aging [35].

2.3 PREVIOUS THERMAL ANALYSIS OF PDAC/PSS AND PAH/PAA FILMS USING MDSC AND QCM-D

Before going any further, a conceptual understanding of how LbL films react to changing temperature is necessary. It was previously proposed by Lavalle *et al.* that the exponential growth of LbL films was the result of polymer chain diffusion "in and out" of the film, while on the other hand linear growth was caused by the inability of this diffusion to occur during the allotted adsorption time period [36]. It would thus be reasonable to assume that films growing in an exponential fashion are more viscoelastic (polymer chains are more mobile) than those growing linearly. Continuing in this vein, one therefore would expect that linearly growing films have a higher T_g than exponentially growing films. In a pair of studies done by Vidyasagar *et al.*, results showed that while the hypothesis proved true for the PDAC/PSS system, it was not directly supportive for the PAH/PAA system [37, 38]. These conclusions were drawn after investigating both PDAC/PSS films assembled at a variety of salt concentrations (0

M, 0.25 M, 0.5 M, and 1.0 M), as well as PAH/PAA films assembled at pH's representative of the four regions mentioned earlier in this paper (pH's of 3.5, 5.5, 7.0, and 9.0). Both studies, in particular their application of the MDSC and QCM-D techniques to study LbL films, will be explored further in the succeeding paragraphs.

Thermal analysis studies via QCM-D for both the PAH/PAA system and the PDAC/PSS system followed the same general procedure [37, 38]. Films were first assembled upon a quartz crystal in the QCM-D cell. Following assembly, a temperature ramping program was initiated. The T_g was taken as the point at which a sudden step increase in ΔD occurred. This sharp change in dissipation is related to a sudden change in film viscoelasticity. It has been proposed that the abrupt increase in ΔD is the result of ion pairs breaking, which in turn leads to chain relaxation (i.e. increased viscoelasticity) [37]. An important consideration when performing thermal analysis via QCM-D is the temperature-dependent response of the bare crystal submerged in water. This is due to the fact that both the density and viscosity of water are functions of temperature, which implies that the submerged crystal response is one as well [39]. In order to account for this, Δf and ΔD values for the bare crystal must be subtracted from the raw data. The results presented in Figure 6 below depict the corrected temperature dependence for both LbL systems investigated by Vidyasagar *et al*. [37, 38]:

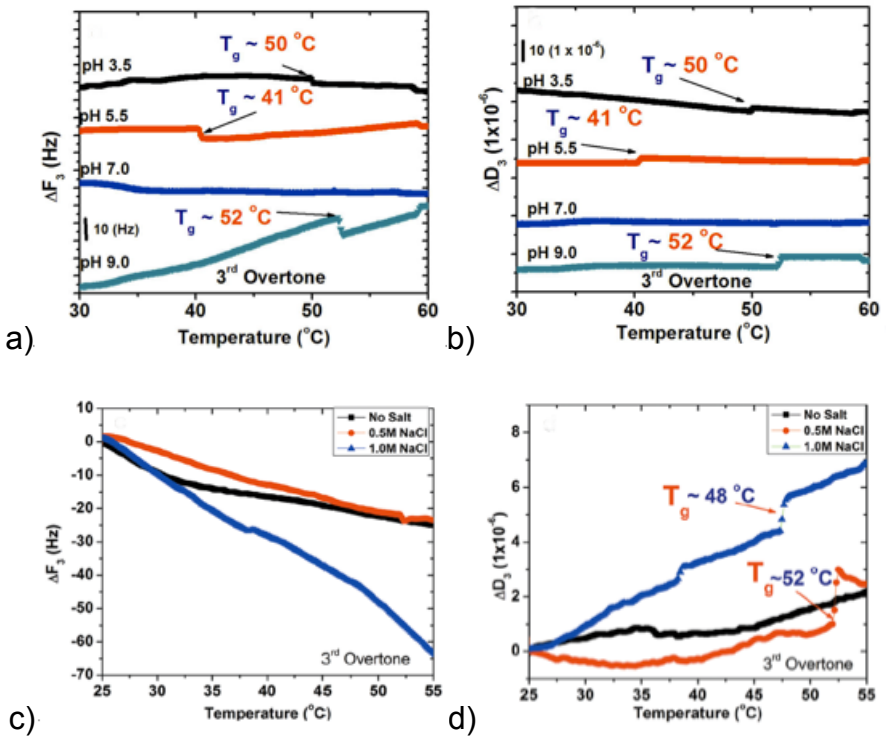

Figure 6. QCM-D thermal analysis data for hydrated LbL films. Parts a) and b) correspond to the PAH/PAA system, while parts c) and d) correspond to the PDAC/PSS system. Note the sharp changes in dissipation signaling a thermal transition. Figure 6a and 6b was reprinted (adapted) with permission from (Vidyasagar, A.; Sung, C.; Losensky, K.; Lutkenhaus, J. L. *Macromolecules.* **2012,** *45,* 9169.). Copyright (2014) American Chemical Society. Figure 6c and 6d was reprinted (adapted) with permission from (Vidyasagar, A.; Sung, C.; Gamble, R.; Lutkenhaus, J. L. *ACS Nano.* **2012,** *6,* 6174.). Copyright (2014) American Chemical Society.

As seen in Figure 6a and 6b above, the QCM-D data for PAH/PAA films typically depicts an increase in Δf during the temperature ramp (excluding the case where pH was 7.0), meaning that the film's water content decreases with increasing temperature. The Δf will drop rapidly when the T_g occurs (once again excluding where pH was 7.0), indicating a quick influx of water into the film. It was reported that for films assembled from pH values of 5.5, 7.0, and 9.0 the ΔD values stayed fairly constant

over the temperature ramp, while for the films assembled at a pH of 3.5 the ΔD values greatly decreased. For all pH values examined with the exception of pH 7.0, an abrupt increase in ΔD was observed; this sharp increase was called the glass transition temperature. On the other hand, PDAC/PSS films (Figure 6c and 6d) displayed a gradual decrease in Δf upon heating for all ionic strengths, indicating an increase in film hydration. There was no abrupt change in Δf reported at the T_g. The ΔD generally exhibited a slight increase over the temperature range examined. Glass transitions were observed to occur for all ionic strengths except for 0 M NaCl. These transitions were weak for the 0.25 M case, but quite distinct for 0.5 M and 1.0 M. It was proposed that the reason why films assembled at an ionic strength of 0.25 M exhibit such a weak transition is because that salt concentration lies near the junction between linear and exponential growth [37].

A useful aspect of QCM-D for thermal analysis is that it is capable of probing Δf and ΔD values at various points throughout the film by means of different overtones. The different harmonics often used in a QCM-D experiment range from the third overtone to the thirteenth overtone, with the third overtone probing deep within the film and the thirteenth overtone corresponding to the region near the crystal film interface. The data for both of the film systems shown in Figure 6 is associated with the third overtone. Analysis for the PAH/PAA system was strictly limited to this overtone, while the study on the PDAC/PSS system incorporated the thirteenth overtone into its analysis as well (data on that overtone not shown). It was reported that this thirteenth overtone exhibits the same transitions as seen in the third overtone, however the transition

magnitudes observed were much larger. This indicates that the T_g in PDAC/PSS films must be more pronounced closer to the film-crystal interface [40, 41].

A well-documented phenomenon worthy of note is the so-called "odd-even" effect. [26, 27, 42, 43] As reported earlier in this paper, this effect refers to the drastic variations in temperature response observed for PDAC/PSS LbL capsules depending on which polyelectrolyte is the terminating layer. The QCM-D study by Vidyasagar *et al.* mentioned above corroborates the earlier experiments describing this effect, for it was seen that films terminated with PDAC swell (Δf decreases and ΔD increases), while those terminated with PSS shrank (Δf increases and ΔD decreases) [37]. The swelling is attributed to electrostatic repulsive forces within the positively-charged, PDAC-terminated film, while the shrinking is due to unfavorable polymer-water interactions for the neutral PSS-terminated film. Figure 7 below illustrates the competition between these electrostatic and hydrophobic forces in the case of PDAC/PSS capsules [26]:

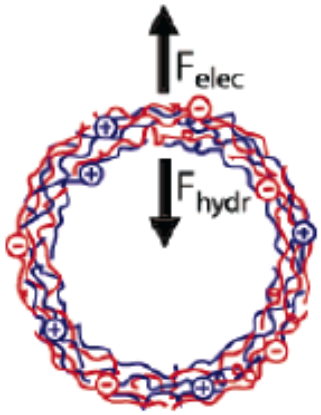

Figure 7. A depiction of the observed competition between electrostatic and hydrophobic forces in PDAC/PSS capsules. Reprinted (adapted) with permission from (Köhler, K.; Möhwald, H.; Sukhorukov, G. B. *J. Phys. Chem. B.* **2006,** *110,* 24002.). Copyright (2014) American Chemical Society.

Interestingly, there was no such "odd-even" effect observed in the QCM-D study on the PAH/PAA system [38].

In order to corroborate the above-mentioned QCM-D findings, MDSC experiments were performed on dry and hydrated films for both sets of LbL systems. Studies by both Vidyasagar *et al.* and Shao *et al.* showed that there is no T_g observed for dry films in either system [30, 37, 38]. However as seen in Figure 8 below, T_g's were indeed observed for hydrated PAH/PAA and PDAC/PSS films [37, 38]:

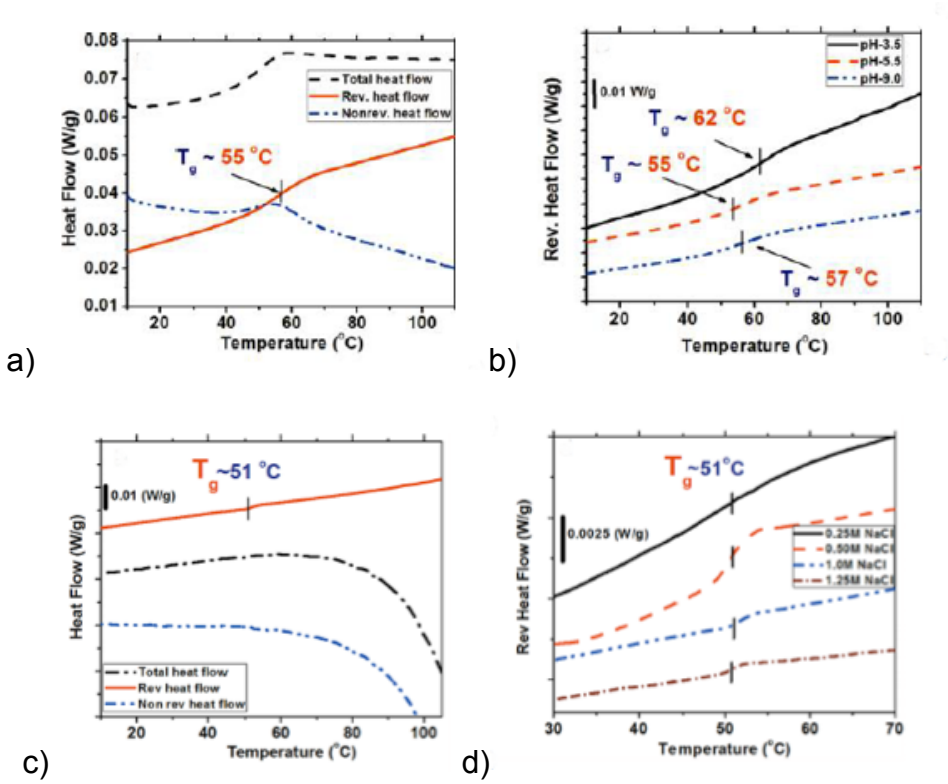

Figure 8. MDSC thermal analysis data for hydrated LbL films. Parts a) and b) correspond to the PAH/PAA system, while parts c) and d) correspond to the PDAC/PSS system. Figure 8a was reprinted (adapted) with permission from (Vidyasagar, A.; Sung, C.; Losensky, K.; Lutkenhaus, J. L. *Macromolecules*. **2012,** *45,* 9169.). Copyright (2014) American Chemical Society. Figure 8b was reprinted (adapted) with permission from (Vidyasagar, A.; Sung, C.; Gamble, R.; Lutkenhaus, J. L. *ACS Nano.* **2012,** *6,* 6174.). Copyright (2014) American Chemical Society.

As seen in Figure 8a and 8b, hydrated PAH/PAA films assembled from polymer solutions of pH 3.5, 5.5, and 9.0 exhibited T_g's. The transition values were actually much higher than those obtained with QCM-D, a fact attributed to the different methods of preparation for the films (i.e. dip vs. flow) [44]. In the case of the hydrated PDAC/PSS films (Figure 8c and 8d), the T_g's showed no variation amongst the different ionic strength conditions. Therefore Vidyasagar *et al.* proposed that MDSC is far less

sensitive to thermal transitions in LbL films [37]. Interestingly, there was no “odd-even” effect observed for the PDAC/PSS films with MDSC. This was attributed to the fact that much thicker films (a couple of microns) are used for MDSC compared to the thin films studied with QCM-D (a couple hundred nanometers), and thus the effect must not be as prominent [37].

3. CURRENT WORK

3.1 INTRODUCTION

Layer-by-layer (LbL) assembly, a process by which nanoscale films are made through the alternating adsorption of oppositely charged species, was first demonstrated by Iler et al. in the mid-1960's, but largely forgotten until a publication by Decher *et al.* in the early 1990's [1, 2]. Since its re-introduction over twenty years ago this cost-effective technique has been proven viable across a diverse array of materials, and as such has found use in a host of applications ranging from optics to drug delivery [3-8]. This technique owes much of its popularity to that fact that through simple adjustment of parameters such as ionic strength, salt type, pH, solvent quality, temperature, and humidity, precise control of film growth and properties can be exercised [8-20].

Despite these benefits, much remains to be learned about the thermal behavior of LbL films, particularly regarding the glass transition temperature (T_g). Clearly this is an important issue considering that the viability of LbL films in certain applications depends on whether they are glassy or rubbery. Seeing as that LbL films are so thin, thermal characterization can be an especially difficult task however. In the past few years a number of thermal characterization techniques have been utilized in an attempt to study LbL films, including microdifferential scanning calorimetry (micro-DSC), swelling/shrinking of LbL capsules, and NMR spectroscopy [26, 43, 45].

Recently, our group has demonstrated that T_g's in LbL films can be measured via quartz crystal microbalance with dissipation (QCM-D) [37, 38]. QCM-D differentiates itself from other potential thermoanalytical techniques by its capacity to observe changes in both hydrated film mass and viscoelasticity as a function of film depth. The great sensitivity of these measurements has proven quite useful in accurately detecting weak transitions. Using QCM-D, we have previously examined hydrated LbL films of both strong and weak polyelectrolyte systems, namely poly(diallyldimethylammonium chloride)/poly(styrene sulfonate) (PDAC/PSS) and poly(allylamine hydrochloride)/poly(acrylic acid) (PAH/PAA) respectively [37, 38]. In the case of the former system, it was found that such films lack a T_g when growing linearly (assembled without salt), while exponentially growing films (assembled with salt) do indeed possess a distinct T_g. These results complemented a hypothesis proposed by Lavalle *et al.*, which stated that linearly growing films are rigid with restricted polymer segmental mobility (and thus have a higher T_g), while exponentially growing films will have greater polymer segmental mobility [36]. For the latter LbL system studied, no such dependence on linear versus exponential film assembly was noted. It therefore was proposed that the thermal properties of PAH/PAA LbL films must be due to a complex interplay of factors such as film composition, hydration, linear or exponential growth, and free volume.

In this particular study, we have applied both QCM-D and modulated DSC (MDSC) to investigate the thermal properties of hydrated PDAC/PSS LbL films into which layers of negatively charged SiO_2 and Laponite (LAP) nanoparticles have been inserted. There have been numerous reports detailing the assembly and potential

applications of such films, but the extent to which these nanoparticles influence film properties is not well known [46, 47]. Of particular interest were the effects that both nanoparticle morphology (spherical vs. platelet) and location (near film-substrate interface vs. within the bulk vs. near the film free surface) have on the previously measured thermal transitions in PDAC/PSS LbL films. Based on existing thermal analysis data involving traditional polymer nanocomposites, one would expect that the observed glass transition temperatures for the PDAC/PSS system to increase for both morphological cases [48]. This phenomenon occurs due to the reduced mobility of the polymer chains in addition to attractive polymer-nanoparticle interactions. In the work presented here, we illustrate that this theory does indeed hold true for polymer-nanoparticle LbL films. For both nanoparticle morphologies, the observed T_g's occurred at values higher than those previously reported for neat PDAC/PSS films. There was little difference noted between the transition values for the two particular morphologies however. Additionally, it was discovered that nanoparticle location within the film does in fact play a role in the observed T_g. In particular, for film configurations where the nanoparticles were added during the middle bilayer, the highest glass transition temperatures were observed. This fact was attributed to the increased available nanoparticle surface area with which neighboring polymer chains could form bonds.

3.2 EXPERIMENTAL

Materials: Poly(diallyldimethylammonium chloride) (PDAC, Mw = 350 000 g mol^{-1}) and poly(styrene sulfonate sodium salt) (PSS, Mw = 500 000 g mol^{-1}) were purchased from Sigma Aldrich and Scientific Polymer Products, respectively. Poly(ethylene imine) (PEI, Mw = 25 000 g mol^{-1}) was purchased from Polysciences, Inc. Laponite RD (LAP, diameter range of 10 to 1000 nm, thickness of 1 nm) was purchased from Southern Clay, while Ludox TM-40 (40 wt % SiO_2 suspension in water, average particle size of 22 nm, and specific surface area of 140 m^2 g^{-1}) was purchased from Sigma-Aldrich. Teflon® and quartz crystal substrates were purchased from McMaster Carr and Q-Sense, respectively.

Preparation of Free-Standing Layer-by-Layer Assemblies: PDAC and PSS solutions were made from their respective homopolymers and 18.2 MΩ Milli-Q water at a concentration of 1 mg mL^{-1}. The concentrations of the SiO_2 and LAP nanoparticle solutions were both adjusted to 0.03 wt %. LbL assemblies were constructed using an automated slide stainer (HMS series, Carl Zeiss, Inc.). The Teflon® substrates used to fabricate free-standing LbL assemblies were cleaned using sonication for 15 min in ethanol, followed by 15 min sonication in deionized water. Teflon® substrates were dipped in PDAC solution for 15 min, followed by three separate rinses with Milli-Q water for 2, 1, and 1 min, respectively. The substrates were then dipped in PSS solution for 15 min, followed by another series of water rinses as before. Whenever the inclusion of a nanoparticle (NP) layer was required, the NP solution would take the position of

PSS in the assembly process. The ionic strength of assembly for all baths was 0.5 M NaCl in order for comparisons to be made with a previous study by our group [37]. The free-standing films that were assembled can be generalized using the following notation: $(PDAC/PSS)_{149}(PDAC/NP)_1$, $(PDAC/PSS)_{74}(PDAC/NP)_2(PDAC/PSS)_{74}$, and $(PDAC/NP)_1(PDAC/PSS)_{149}$. These configurations were chosen so as test the effect that NP location has on the film's glass transition temperature (i.e. near the film-substrate interface, bulk, or film free surface). The LbL films were then dried in ambient air and stored in a desiccator until further use. The films were isolated from their Teflon® substrates just before MDSC experiments.

Preparation of Layer-by-Layer Assemblies via Quartz Crystal Microbalance with Dissipation (QCM-D): All QCM-D experiments were performed using the Q-Sense E1 system. The gold-plated AT-cut quartz crystals were first plasma treated for 10 min followed by a 10 min immersion in a water/NH_4OH/H_2O_2 (5:1:1) mixture at 70 °C, dried using nitrogen, and then plasma treated as before. LbL film assembly was then carried out by first flowing 1 mg mL^{-1} PEI solution (pH 4.5) for 15 min, followed by a 5 min rinse using Milli-Q water (pH 4.5). This initial layer was considered the zeroth layer and was used as a baseline for all QCM-D experiments. Then, 0.1 mg mL^{-1} PSS solution was passed over the crystal at a flow rate of 200 μL min^{-1} for 15 min, followed by a 5 min rinse using 0.5 M NaCl. Next, 0.1 mg mL^{-1} PDAC solution was passed for 15 min, followed by rinsing as before. Whenever a nanoparticle layer was required, 0.0015 wt % solutions of either SiO_2 or LAP were passed over the crystal for 15 min, followed by a 5 min rinse as previously described. The assembled films can be generalized using the

following notation: $PEI(PSS/PDAC)_6(NP/PDAC)_1$, $PEI(PSS/PDAC)_3(NP/PDAC)_1(PSS/PDAC)_3$, and $PEI(NP/PDAC)_1(PSS/PDAC)_6$. These configurations were chosen so as test the effect that NP location has on the film's glass transition temperature (i.e. near the film-substrate interface, bulk film, or film free surface). With the exception of the PEI solution, all polymer and nanoparticle solutions used during the assembly process were at an ionic strength of 0.5 M NaCl. This enabled comparisons to be made with a previous study by our group [37].

Thermal Analysis of Layer-by-Layer Assemblies via QCM-D: Thermal analysis of hydrated layer-by-layer assemblies using QCM-D was achieved by means of a temperature program created with the QSoft Software (Q-Sense). Heating cycles were performed at a rate of 1 °C min^{-1} over temperatures ranging from 25 to 71 °C. In order to keep the films in a hydrated state throughout the entire analysis, a 0.5 M NaCl solution was continually passed through the cell at a flow rate of 200 μL min^{-1}.

Quantification of QCM-D Data: The Sauerbrey equation, which relates change in frequency and the adsorbed mass, was found to inadequately describe the films analyzed in this study [33]. For viscoelastic films such as the ones used here, more complex models have to be employed to capture changes in both frequency and dissipation. We used the frequency-dependent extended Voigt model to study LbL film growth. The QTools modeling software (Q-Sense) took all overtones (n = 3-13) into consideration. Table 1 below lists the parameters that were used in the modeling process:

Table 1. Fitted Parameters Used for Extended Voigt Modeling Process

Parameters to Fit:	*Minimum*	*Maximum*	*Step (Iterations)*
L1 Viscosity (kg m^{-1} s^{-1})	0.0001	0.01	50
L1 Shear (Pa)	100	1E12	21
L1 Thickness (m)	9.5238E-11	1E-6	21
L1 Viscosity Frequency	-2	0	10
L1 Shear Frequency	0	2	10

Additionally, the fixed parameters utilized during for these models were: fluid
(kg m^{-3}) of 1000, fluid viscosity (kg m^{-1} s^{-1}) of 0.001, and L1 density (kg m^{-3}) (

Modulated Differential Scanning Calorimetry Measurements (MDSC):
was performed on film samples in a heat-cool-heat cycle. These film samples v
hydrated in 12 wt % of the 0.5 M NaCl assembly solution and weighed betwee
15 mg, depending on sample availability. Tzero hermetic pans and lids were us
Hydrated films were ramped from 0 to 115 °C at a rate of 2 °C min^{-1} with amp
1.272 °C for a period of 60 s. All transitions reported were taken from the secc
heating cycle.

3.3 RESULTS AND DISCUSSION

We performed experiments on PDAC/PSS LbL films assembled from s
of 0.5 M NaCl where nanoparticles of either spherical or platelet morphology v
inserted at varying intervals (Figure 9).

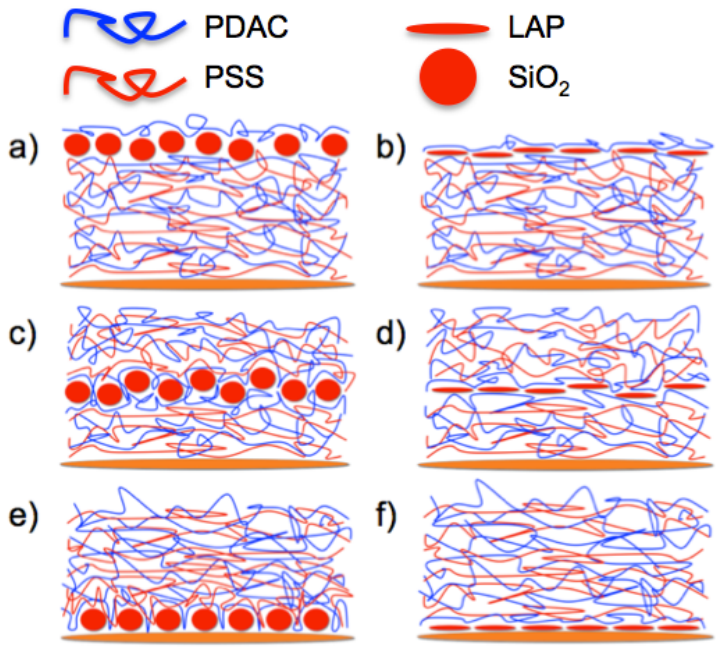

Figure 9. The various film configurations studied in this work. Parts a), c), and e) correspond to films incorporating SiO_2 nanospheres, while parts b), d), and f) correspond to films incorporating LAP nanoplatelets.

Polyethyleneimine (PEI) was utilized as an initial layer in order to promote adsorption. Our motivation was to determine how both nanoparticle morphology and relative location within the film influences T_g. As the films were assembled within the QCM-D cell, frequency (Δf) and dissipation (ΔD) values were simultaneously recorded. A decrease in Δf indicates that mass is being adsorbed, while an increase in ΔD means the film viscoelasticity is increasing. The extended Voigt model was applied in modeling the assembly data, and the resulting fits enabled the determination of thickness for all the various film configurations. It was observed that the fit began to deviate from the experimental data following the addition of the nanoparticle layer, in other words the film properties have significantly changed. This deviation was considerably more

prominent for the 13th overtone data as opposed to the 3rd overtone data. Figures 10 and 11 depict both the raw and fitted (solid black line) assembly data for the nanoparticle morphologies tested via QCM-D.

As previously shown by our group, individual layer adsorption of an exponentially growing, neat PDAC/PSS film assembled from 0.5 M NaCl solutions is typified by step-wise decreases in Δf. Additionally, ΔD will increase upon adsorption of the first layer, followed by an oscillation over a constant value [37]. The insertion of either spherical SiO_2 or platelet LAP nanoparticles during assembly results in markedly different assembly behaviors from that of the neat film. Figure 10 corresponds to both the 3rd and 13th overtone measurements for PDAC/PSS films that incorporate SiO_2. It is clearly seen for all film conformations, that the step during which SiO_2 is added will lead to large decreases in Δf as well as large increases in ΔD. Interestingly, for the particular conformations where SiO_2 is added either within the first or middle bilayers, dissipation is observed to decrease for the remainder of the experiment. This makes sense if one imagines the nanospheres slowly embedding themselves in the film, thereby leading to film densification. SiO_2 embedment in a PDAC layer is not an unusual phenomenon, being previously observed by Xu *et al*. [49]. In their experiments a single layer of PDAC was deposited on a QCM-D crystal, followed by a layer of SiO_2 nanospheres. Significant reductions in ΔD were observed over the course of several hours, an occurrence attributed to surface rearrangements between the reptating PDAC chains and the SiO_2 nanospheres (i.e. a denser and more rigid film results).

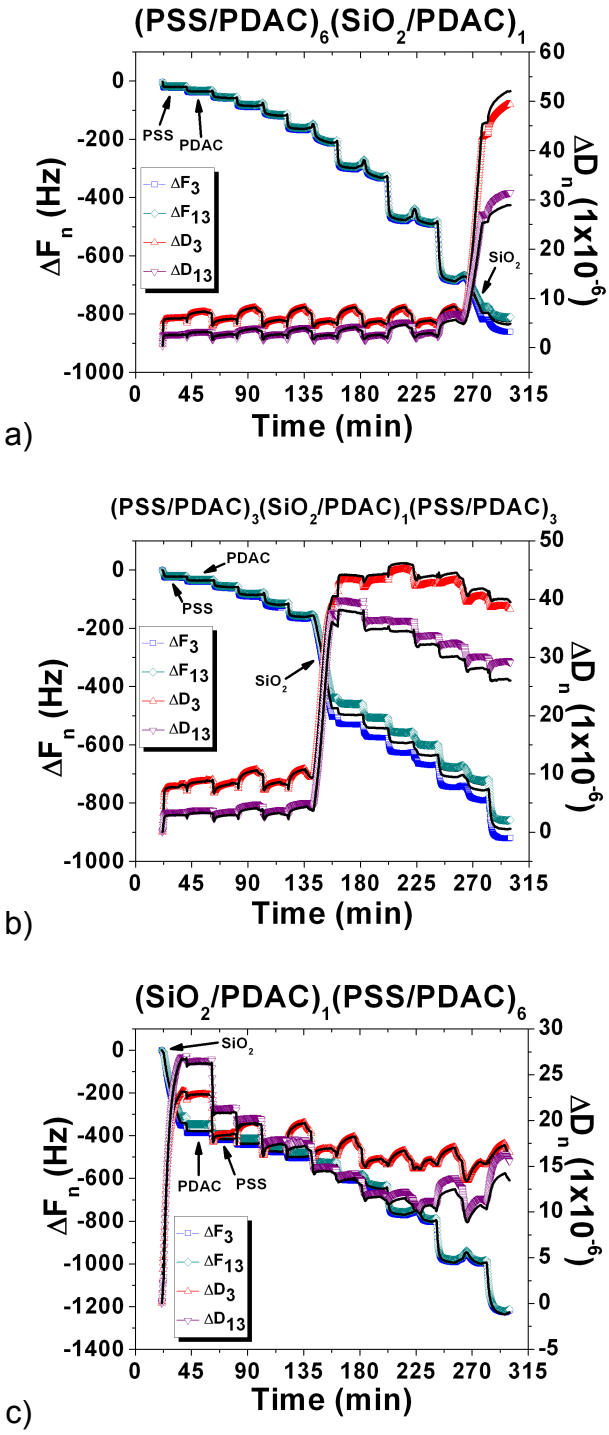

Figure 10. Raw and fitted (black line) data for the 3rd and 13th overtones of PDAC/PSS films incorporating SiO_2. Part a) corresponds to films where SiO_2 was added within the last bilayer, part b) correspond to films where SiO_2 was added in central bilayer, and part c) corresponds to films where SiO_2 was added within the first bilayer.

Figure 11 corresponds to both the 3rd and 13th overtone measurements for PDAC/PSS films that incorporate LAP. Upon adsorption of the LAP layer, very little change in both frequency and dissipation are observed. The only case in which there is a notable increase in frequency and a decrease in dissipation observed occurs when LAP is added during the first adsorption step. This could be because LAP adsorbs more favorably onto the PEI-coated crystal than onto the PDAC layer.

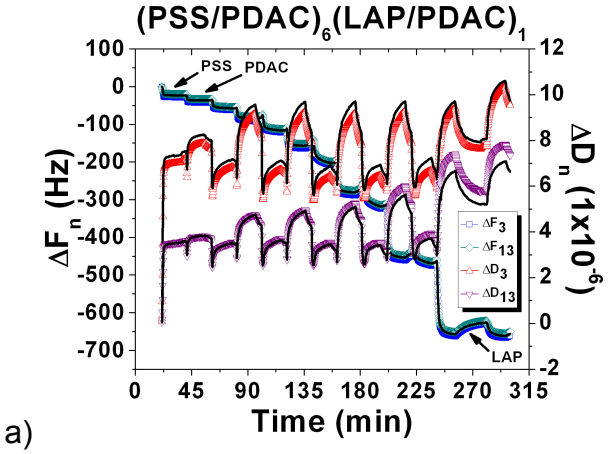

a)

Figure 11. Raw and fitted (black line) data for the 3rd and 13th overtones of PDAC/PSS films incorporating LAP. Part a) corresponds to films where LAP was added within the last bilayer, part b) corresponds to films where LAP was added in central bilayer, and parts c) corresponds to films where LAP was added within the first bilayer.

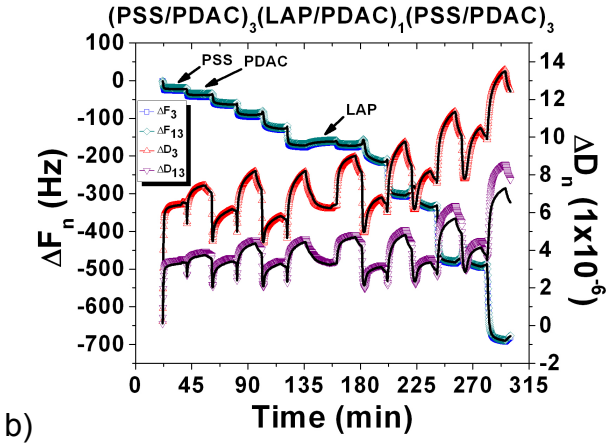

b)

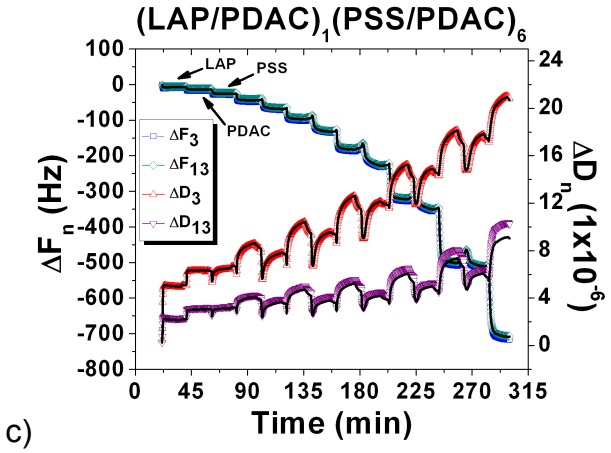

c)

Figure 11. Continued.

After the completion of the LAP addition step, subsequent layer adsorption results in a continually increasing trend in dissipation for the remainder of the assembly experiment. A potential explanation for this occurrence is that the rigid LAP layer in effect creates two mutually exclusive regions of the film. Thus as the quartz crystal oscillates, the portion of the film below the LAP layer will move in a direction opposite to that of the remaining film above. A diagram explaining this phenomenon is shown in Figure 12.

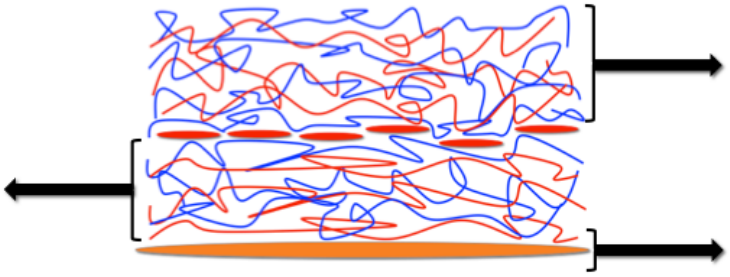

Figure 12. Illustration of the unique viscoelastic behavior in LAP-containing PDAC/PSS films. In this diagram, negatively charged LAP nanoplatelets are shown as forming a rigid, densely packed layer. We argue that this layer isolates the viscoelastic portions from one another, thereby causing the continually increasing dissipation values as assembly progresses.

As previously mentioned, due to the ineffectiveness of the Sauerbrey Model in accurately describing viscoelastic films such as those assembled here, the extended Voigt model was required. Figure 13 illustrates the film thicknesses that were obtained via this modeling process.

Figure 13a corresponds to the various film arrangements that incorporated SiO_2 nanospheres. The thickest film results when SiO_2 is added in the first layer. It is assumed that the addition of the nanosphere layer interrupts the exponential growth associated with this polyelectrolyte system, thereby preventing thicker films from assembling for the remaining film configurations. It is interesting to note that the thickness associated with the SiO_2 layer decreases when it is added later in the assembly process. When added within the first or middle layer pairs a thickness increase of nearly 50 nm is observed, implying that multiple layers of SiO_2 nanospheres (~22 nm in diameter) are adsorbed. However the film thickness increases by no more than 10 nm whenever the

SiO_2 nanospheres are added during the final bilayer. This small thickness increase could be explained in two ways. One potential explanation is that exponentially growing films have more loops and trains (i.e. greater free volume), and thus the nanospheres would be able to nestle into the film bulk rather easily. The other explanation could be that patchy adsorption of SiO_2 occurs, as opposed to the laterally homogenous layers observed in the other configurations.

Figure 13b corresponds to the different film configurations including LAP. It turns out that the three films incorporating LAP all conclude with roughly the same thickness, a thickness that is significantly smaller than the neat $(PSS/PDAC)_7$ film. This reduced thickness is to be expected if the addition of the LAP nanoplatelet layer indeed interrupts the exponential growth associated with this polyelectrolyte system. Additionally, LAP nanoplatelets, which are only about 1 nm in thickness, have been shown to adsorb parallel to the film surface and thus will not contribute to the film thickness in any significant fashion [47].

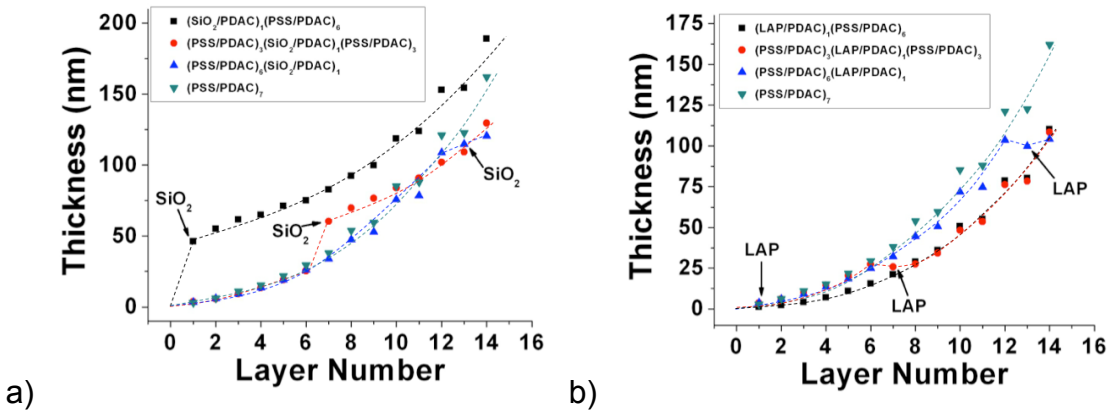

Figure 13. Film thicknesses for PDAC/PSS films incorporating nanoparticles of either spherical or platelet morphologies. Part a) depicts SiO_2-containing films while part b) depicts LAP-containing films. These thicknesses were determined by means of the extended Voigt model. Dotted lines have been included to "guide" the eye.

Following assembly, temperature-controlled QCM-D was used to observe changes in frequency and dissipation for all conformations of the nanoparticle-incorporating PDAC/PSS films. This involves first submerging the LbL films in water of ionic strength matching their assembly conditions and then allowing a computer program to ramp the QCM-D cell from 25 to 70 °C at 1 °C min^{-1}. Both density and viscosity of water are functions of temperature, and as a result they will influence the submerged crystal response [39]. Thus in order to properly isolate the response of the LbL film, a temperature-dependent response of the bare crystal must be subtracted from the raw data. This subtraction procedure generates the "corrected data" shown in both Figures 14 and 15.

A very useful feature of QCM-D, especially in terms of thermal analysis, is its capability to determine Δf and ΔD values at various points throughout the film by means

of overtones. Each particular overtone has an associated penetration depth dependent upon the decay length of the evanescent wave in contact with the film and bulk fluid. This depth decreases with increasing overtone number, meaning that lower overtones are more ideally suited for probing the film-fluid interface, while the higher overtones are better at investigating the film-substrate interface [40, 41]. For example in pure water at 20 °C, this penetration depth is roughly 145 nm for the 3rd overtone, but just 50 nm for the 13th overtone.

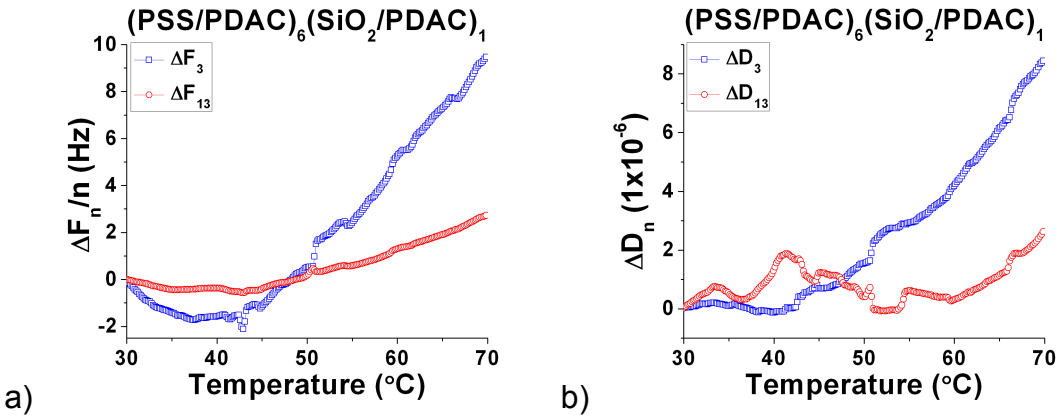

Figure 14. The "corrected data" for the 3rd and 13th overtones for PDAC/PSS films incorporating SiO_2. Parts a) and b) correspond to films where SiO_2 was added within the last bilayer, parts c) and d) correspond to films where SiO_2 was added in central bilayer, and parts e) and f) correspond to films where SiO_2 was added within the first bilayer. Note the abrupt decreases in frequency and increases in dissipation for the film show in parts c) and d). These changes are indicative of a thermal transition occurring within the film.

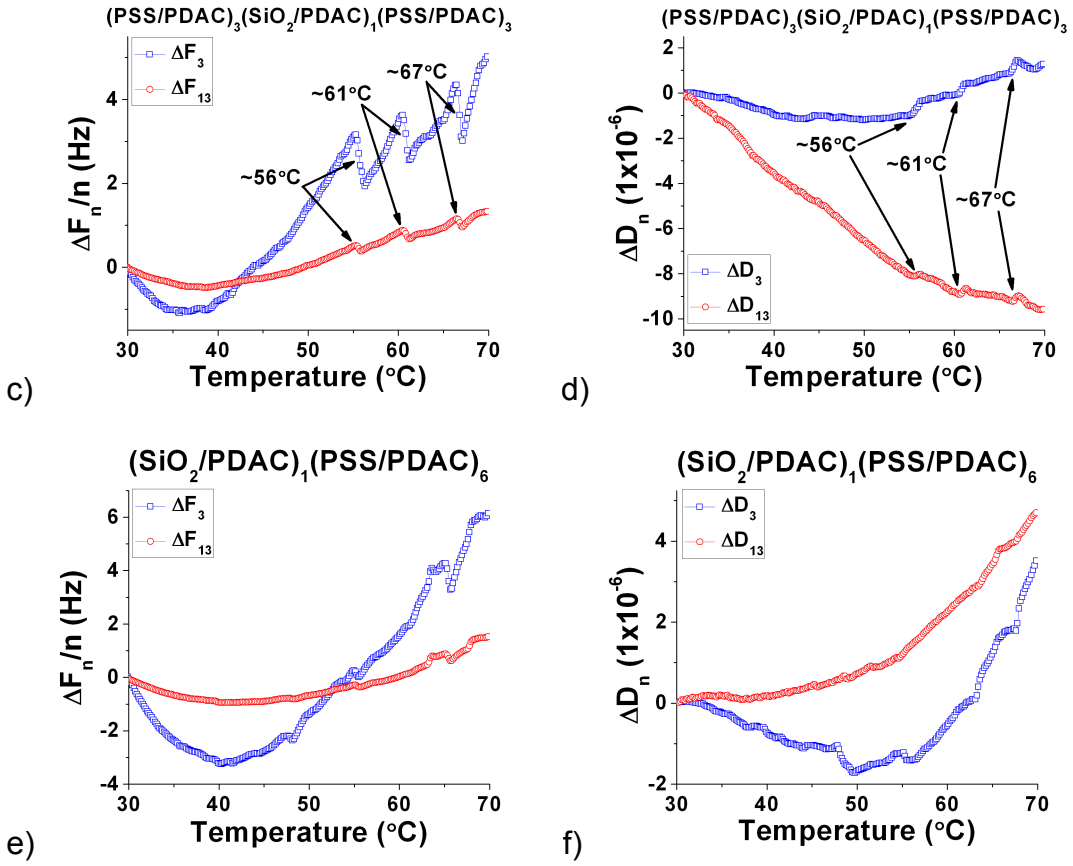

Figure 14. Continued.

In general, for films that incorporate SiO_2 nanospheres (Figure 14), the Δf values were observed to gradually increase with increasing temperature. This corresponds to the water exiting the film. Contrary to expectation, ΔD values also typically increased over the course of the temperature scan, seeming to indicate that the films were becoming more viscoelastic with decreasing hydration. Glass transitions were solely observed in the case of the $(PSS/PDAC)_3(SiO_2/PDAC)_1(PSS/PDAC)_3$ film configuration (Figure 14c and 14d). This is potentially due to the increased available nanosphere surface area with which polymer chains could form bonds. In Figure 14c the Δf values were observed to

abruptly decrease at 56, 61, and 67 °C, illustrating a sudden influx of water into the film. Correspondingly, there were also abrupt increases in ΔD values at these same temperatures, implying an increase in film viscoelasticity. The transition at 56 °C corresponds to the T_g previously assigned to neat PDAC/PSS film, albeit slightly elevated due to the presence of the nanosphere layer. The latter two transition temperatures correspond to the polymer chains in immediate proximity with the nanospheres. In a previous study on the thermal properties of hydrated PDAC/PSS films, we observed a larger dissipation response from the 13^{th} overtone. This showed that there was actually a more prominent transition near the film-substrate interface for neat PDAC/PSS films [37]. As seen in Figure 14c and 14d, this was not observed here, rather it seems that the 3^{rd} overtone registers more prominent transitions. This may simply be due to the nanoparticles dampening the response of the 13^{th} overtone; not unreasonable when one considers that higher overtones have lower signal-to-noise ratios.

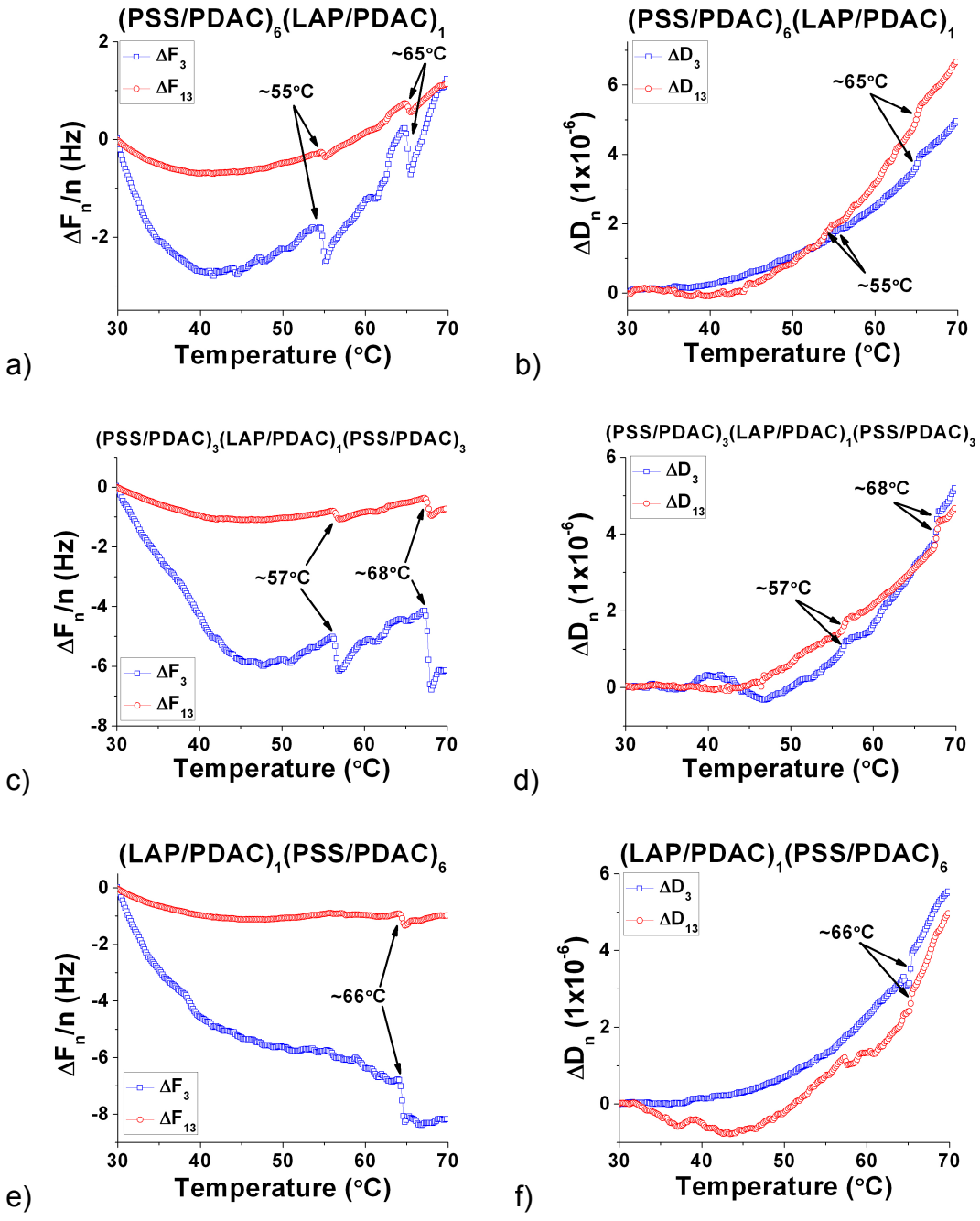

Figure 15. The "corrected data" for the 3rd and 13th overtones for PDAC/PSS films incorporating LAP. Parts a) and b) correspond to films where LAP was added within the last bilayer, parts c) and d) correspond to films where LAP was added in central bilayer, and parts e) and f) correspond to films where LAP was added within the first bilayer. Note the abrupt decreases in frequency and increases in dissipation seen in all cases. These are indicative of a thermal transition occurring within the film.

Typically, for films that incorporate LAP nanoplatelets (Figure 15), the Δf values tended to exhibit a slight decrease with increasing temperature. This corresponds to the water entering the film. Reflecting this, ΔD values increased over the course of the temperature scan, indicating that the films were becoming more viscoelastic with increasing hydration. Unlike for the films incorporating SiO_2, there were T_g's observed for all LAP film configurations. For the case of the $(PSS/PDAC)_6(LAP/PDAC)_1$ film (Figure 15a and 15b), two abrupt drops were observed in the Δf data set, one at roughly 55 °C and the other at about 65 °C. Concurrently, there were also slight jumps in ΔD at the same temperatures. For the $(PSS/PDAC)_3(LAP/PDAC)_1(PSS/PDAC)_3$ film (Figure 15c and 15d) abrupt drops are observed for Δf at roughly 57 and 68 °C. Similarly, the ΔD data is marked by slight jumps at those same temperatures. For both of the above film types, the lower transitions (55 and 57 °C respectively) correspond to the T_g previously observed for neat PDAC/PSS films, perhaps slightly elevated due to the presence of the nanoplatelet layer. On the other hand, the higher transitions (65 and 68 °C respectively) correspond to the polymer chains in close proximity to the LAP nanoplatelets. In the case of the last LAP film configuration, $(LAP/PDAC)_1(PSS/PDAC)_6$, Δf data values (Figure 15e) depict a sharp drop 66 °C, while ΔD (Figure 15f) exhibits a corresponding increase at the same temperature. It appears that the entire film must therefore exhibit the same elevated thermal properties for this particular film configuration. As was the case with SiO_2 films, the transitions observed for LAP films were actually more prominent toward the film-liquid interface, i.e. the 3rd overtone.

The goal of this study was to utilize the QCM-D technique in order to determine the roles that both nanoparticle morphology and layer location play in influencing the T_g's observed for PDAC/PSS films. We previously have defined a T_g observed via QCM-D as being rather abrupt changes in both Δf and ΔD [37]. These changes correspond to the breaking and relaxing of ion pairs, followed by chain relaxation (in other words, increased viscoelasticity). As discussed earlier, all observed T_g's, regardless of nanoparticle morphology, were elevated with respect to those found in neat PDAC/PSS films. There was little difference observed between the transition values for the two particular morphologies. The main distinction was that normally two T_g's were observed for LAP-containing films, while three such transitions were noted for the SiO_2-containing films. We believe that the lower transition temperature corresponds to the PDAC/PSS layers, while any additional transitions correspond to the polymer in the immediate vicinity of the nanoparticles. The stepwise character of these observed transitions could potentially be due to the surpassing of various weak interaction energy barriers necessary for rearrangement to occur within the nanoparticle layer [50]. Interestingly, it was found that nanoparticle location within the film does indeed influence the observed T_g. In particular, for film configurations where the nanoparticles were added during the middle bilayer, the highest glass transition temperatures were observed. This fact was attributed to the increased available nanoparticle surface area with which nearby polymer chains could form bonds. It is worth mentioning that for all the reported thermal transitions found with QCM-D, while differing in absolute value,

were reproducible in at least two-thirds of all film samples. Table 2 summarizes the results of all the above-mentioned nanoparticle QCM-D thermal analysis tests.

Table 2. T_g Values Obtained via QCM-D for Hydrated PDAC/PSS LbL Films Incorporating Nanoparticles.

LAP Film Configuration	*Averaged Glass Transition Temperature (°C)*
$(PDAC/PSS)_6(PDAC/LAP)_1$	57.1 ± 2.6 64.4 ± 0.7
$(PDAC/PSS)_3(PDAC/ LAP)_1(PDAC/PSS)_3$	58.0 ± 2.0 65.7 ± 2.2
$(PDAC/ LAP)_1(PDAC/PSS)_6$	62.2 ± 1.9
$(PDAC/PSS)_6(PDAC/ SiO_2)_1$	None
$(PDAC/PSS)_3(PDAC/ SiO_2)_1(PDAC/PSS)_3$	56.1 ± 1.6 62.1 ± 1.5 67.7 ± 1.4
$(PDAC/ SiO_2)_1(PDAC/PSS)_6$	None

Modulated DSC (MDSC) was used in an attempt to corroborate QCM-D findings. MDSC differs from conventional DSC in that rather than just a linear temperature ramp, both superimposed sinusoidal and linear temperature profiles are utilized. Therefore it becomes possible to separate overlapping thermal phenomena. The total heat flow measured via MDSC (related to the heat flow from a conventional DSC) is the sum of both the "reversing heat flow" and the "non-reversing heat flow." The former curve contains thermal events that occur quickly, i.e. shorter than the modulation period, and is similar to the sample's heat capacity. Typical thermal events found in this curve are melting and glass transitions. The latter curve corresponds to thermal events that take place over longer time scales, i.e. more slowly than the modulation period. This

is similar to kinetic events like cross-linking, volatilization, and aging [32]. MDSC is normally especially useful for weak transitions, however we have previously discovered that QCM-D is actually more sensitive for observing thermal transitions in hydrated PDAC/PSS LbL assemblies [37].

MDSC scans were performed for bulk nanoparticle-containing PDAC/PSS films that were analogous in configuration to those used in QCM-D experiments. There were no discernable thermal transitions observed for hydrated (12 wt % water) films incorporating SiO_2. It is quite possible that the "hydrated" thermal transitions observed for SiO_2-containing films with QCM-D are just too faint for the MDSC technique to register. In the case of LAP-containing hydrated films however, transitions were observed in roughly fifty percent of all samples. Table 3 summarizes the results of these LAP MDSC tests.

Table 3. T_g Values Obtained via MDSC for Hydrated PDAC/PSS LbL Films Incorporating LAP Nanoplatelets.

LAP Film Configuration	*Averaged Glass Transition Temperature (°C)*
$(PDAC/PSS)_{149}(PDAC/LAP)_1$	46.0 ± 5.8
$(PDAC/PSS)_{74}(PDAC/LAP)_2(PDAC/PSS)_{74}$	55.8 ± 9.0
$(PDAC/LAP)_1(PDAC/PSS)_{149}$	48.4 ± 11.3

The values for these above-mentioned films were all obtained from the second heating cycle. Interestingly, the average glass transition temperatures reported for both the $(PDAC/PSS)_{149}(PDAC/LAP)_1$ and $(PDAC/LAP)_1(PDAC/PSS)_{149}$ films were quite lower than the 51°C transition reported for hydrated, neat PDAC/PSS films. On the other hand,

the $(PDAC/PSS)_{74}(PDAC/LAP)_2(PDAC/PSS)_{74}$ film was observed to have transition temperatures higher than 51 °C, keeping with the trend noted in the QCM-D experiments. However it should be noted that each observed T_g was very broad and weak. In fact, 51 °C was well within the reported standard deviations for all cases. Thus no definitive conclusions can be drawn from these reported transition temperatures found via MDSC.

3.4 CONCLUSION

The thermal properties of hydrated PDAC/PSS LbL films incorporating both spherical (SiO_2) and platelet (LAP) nanoparticles at varying locations have been investigated using MDSC and QCM-D. Using QCM-D we have observed clear, reproducible T_g's in all LAP film configurations and in one particular SiO_2 configuration. All observed T_g's, regardless of nanoparticle morphology, were elevated with respect to those found in neat PDAC/PSS films. In addition, there was little difference noted between the transition values for the two particular morphologies. It was discovered that the highest glass transition temperatures were observed for film configurations where the nanoparticles were added during the middle bilayer. We attributed this phenomenon to the increased available nanoparticle surface area with which nearby polymer chains could form bonds. Unfortunately the extremely weak and broad thermal transitions observed with MDSC proved to be inconclusive in either

supporting or refuting these observations made via QCM-D. Future work will focus on thermal analysis of PDAC/PSS complexes using QCM-D.

4. FURTHER EXPLANATION OF THE QCM-D TECHNIQUE

4.1 DEVELOPMENT OF THE QCM-D TECHNIQUE

Since the late 1800's it has been known that quartz is piezoelectric, meaning that the application of a voltage to a crystal will induce an oscillation at a particular frequency. It was not until the late 1950's however that this material property could be utilized for precise quantitative measurements. Key to this development was Sauerbrey's equation, which showed that mass change, Δm, on the surface of a quartz crystal was related to frequency change, Δf, via the following:

$$\Delta m = -C\left(\frac{\Delta f}{n}\right) \tag{4.1}$$

where C = 17.7 ng cm^{-2} s^{-1} and n refers to crystal overtone number [33]. Sauerbrey's simple relation does make several assumptions however, namely that the mass added is much less than that of the crystal, that the mass is rigidly adsorbed (no slip/deformation caused by oscillating crystal), and that the mass added is evenly distributed. Despite these assumptions, it did not take long for people to realize the usefulness of Sauerbrey's equation. With the help of the quartz crystal microbalance (QCM), it was shown that one could actually determine masses as small as 1 pg cm^{-2} [51]. In the years since then QCM has found use in a wide range of applications, particularly for where monitoring deposition rates of materials onto surfaces is desired.

The next major evolutionary step for QCM was adaptation for operation in the liquid phase. This 'wet' QCM was first shown by Nomura in 1980, and was pioneered

predominantly by Kanazawa and coworkers [52, 53]. One hope was that this would enable the use of QCM in biomedical applications. Unfortunately the Sauerbrey equation is not capable of accounting for dissipation (the sum of all mechanisms that dissipate energy in the oscillating system), and thus QCM has found itself strictly limited to thin, rigid films [54]. Due to the fact that QCM is unable to accurately analyze viscoelastic films (which incorporate aspects of both viscous and elastic materials), a real need was felt for a technique capable of measuring energy dissipation. Finally during the mid-1990's a technique known as quartz crystal microbalance with dissipation (QCM-D) was developed to fill the void [54, 55].

4.2 THEORY

These are other numerous resources available that provide great insight into the theoretical aspects of both QCM and QCM-D [54-56]. Thus, for the purposes of this thesis the scope will be limited to a general overview of the theory.

Quartz is a commonly found crystalline form of silicon dioxide, SiO_2 [57]. There are several phases of quartz available, but the one used for QCM applications is α-quartz, which is stable up to 573 °C. An addition benefit of this particular phase is its piezoelectricity, a property that stems from polarity along one of the symmetry axes [55]. Two cuts of quartz have been used throughout the history of QCM, namely X-cut (cut normal to x-axis) and AT-cut (cut at a 35° angle from the ZX-plane). The former was gradually phased out due to a tendency of frequency to drift with temperature

changes and replaced with the latter, introduced in 1934 and now commonly used in all QCM applications [58]. AT-cut crystals can be induced to undergo a shear strain upon exposure to a voltage, and resonance occurs when the thickness of the crystal is at an odd integer of half wavelengths of the induced shear wave [55].

Due to the fact that both mass and current are oscillating at the same time, the operation of a basic QCM instrument can be visualized by either a mechanical model (Figure 16a) or by an electrical model (Figure 16b) [59].

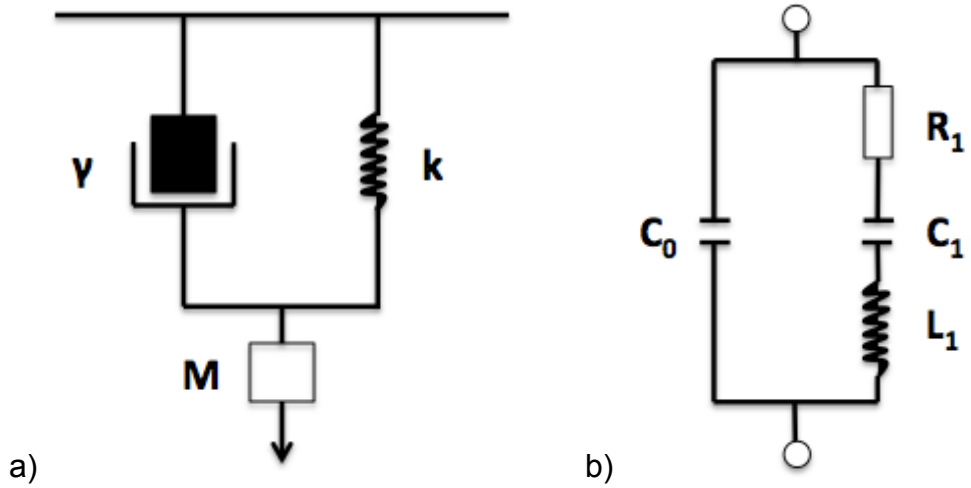

Figure 16. Models commonly used to describe the operation of QCM. Part a) refers to the Mechanical Model Circuit (composed of two elements, namely a spring and a dashpot), while part b) corresponds to the Electrical Model Circuit (composed of four elements, in particular a resistor, two capacitors, and an inductor). Reprinted (adapted) with permission from (Buttry, D.; Ward, M. *Chem. Rev.* **1992,** *92,* 1355.). Copyright (2014) American Chemical Society.

The mechanical model is best suited to painting a picture of the physical interactions between the crystal and the deposited mass. The electrical model on the other hand is useful for explaining the measurement process. The way by these two models can be

related is through the following corresponding terms: the inductance, L_1, is equal to the vibrating mass, M; the motional capacitance, C_1, is equal to $1/k_1$; and the resistance, R_1, is equal to the system losses, γ. C_0, known as the shunt capacitance, is an electrical component stemming from electrode overlap and thus is not present in the mechanical model [59].

As previously described, the unique aspect of QCM-D is the utilization of a dissipation factor, ΔD, which can be expressed via the following equation:

$$\Delta D = \frac{E_{dissipated}}{2\prod E_{stored}} \tag{4.2}$$

where $E_{dissipated}$ is the energy dissipated during one period of oscillation and E_{stored} is the energy stored in the oscillating system [57]. Changes in ΔD are related to the shear viscous losses induced by the adsorbed films, and thus can be especially useful in making structural determinations.

There is also another important detail particular to QCM-D that warrants mentioning – overtones. In traditional QCM, the only overtone measured is that of the resonant frequency (i.e. 5 MHz), but with QCM-D it is possible to record data for numerous overtones (n = 1, 3, 5, 7, 9, 11, and 13). Each overtone is associated with a certain penetration depth, where the n = 3 harmonic probing deep within the film and the n = 13 harmonic corresponding to the film/crystal interface. This is depicted in Figure 17. It is worth noting that the depths shown here correspond to measurements taken in pure water. The actual film thickness the QCM-D can properly handle will depend on film viscoelasticity (which causes damping of crystal oscillations).

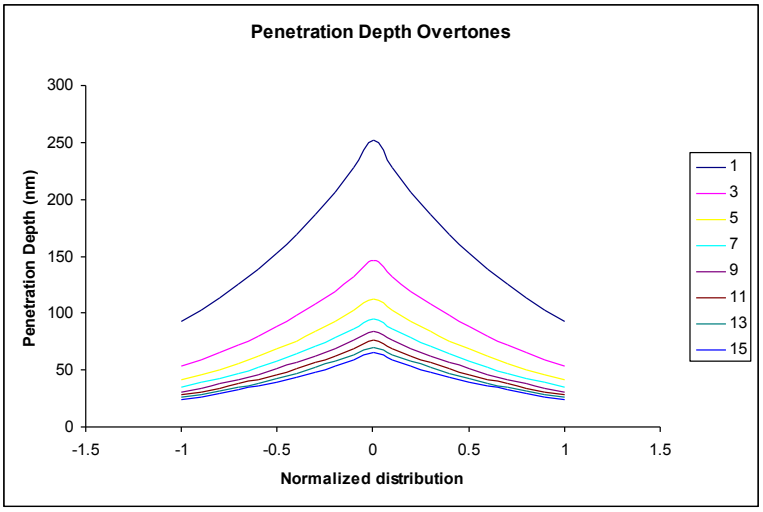

Figure 17. Various overtone penetration depths the can be probed via QCM-D. Note, these values were determined in pure water. Used with permission from Biolin Scientific.

Another interesting consideration regarding overtones is their sensitivity. Sauerbrey showed that the quartz crystal vibration is typically located in the area covered by the two electrodes, also known as the "active area" [60]. As depicted in Figure 18 below, the amplitude of vibration is characterized by a Gaussian function.

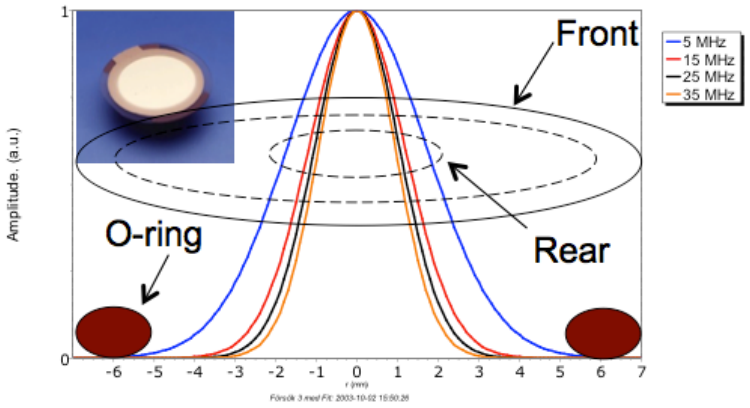

Figure 18. The sensitivity distribution for a typical QCM-D crystal. Note that the distribution narrows with increasing overtone number. Used with permission from Biolin Scientific.

In other words this means that overtones are most sensitive near the crystal center, where the higher the overtone number is, the narrower the sensitivity zone. Additionally the voltage that reaches the QCM-D instrument decreases with increasing overtone number, thus higher overtones will be the first to be lost due to crystal dampening.

In order to measure both Δf and ΔD in a typical QCM-D experiment (Figure 19), first a voltage must be applied to the crystal, allowing it to oscillate.

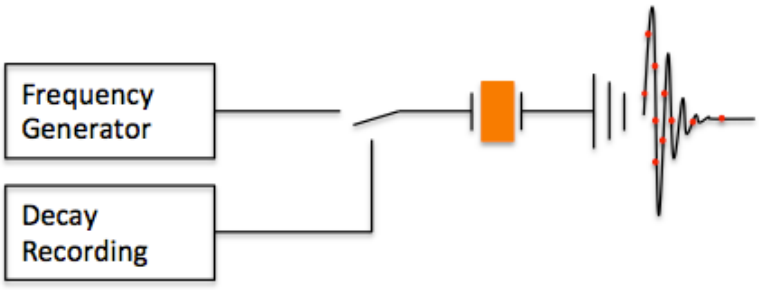

Figure 19. Schematic of the process required for obtaining both Δf and ΔD values using QCM-D. Used with permission from Biolin Scientific.

Then the driving power is cut off and the voltage over the crystal decays as an exponentially dampened sinusoidal:

$$A(t) = A_0 e^{t/\tau} \sin(2\pi f t + \varphi) \tag{4.3}$$

where τ is the decay time constant, f is the frequency, and φ is the phase angle [54]. The decay constant can be related to the dissipation factor via the following equation [54]:

$$\Delta D = \frac{1}{\pi f \tau} \tag{4.4}$$

Measurements done via QCM-D can be acquired very quickly as a result of there only being one decay recording necessary to determine both Δf and ΔD [61]. It is these rapid acquisition rates that make possible the observation of multiple overtones. As an example of the high acquisition times possible with QCM-D, the particular E1 QCM-D model used in this thesis work is capable of recording data of 13 separate harmonics at a rate of 200 times per second.

4.3 QCM-D DATA ANALYSIS

In the rare cases when ΔD equals zero, the Sauerbrey model is perfectly applicable for analysis of QCM-D data. In fact, Sauerbrey may remain a sufficiently approximation as long as the observed ΔD values are no higher than 5-10% of observed Δf values. Technically however, once viscoelastic behavior begins in the adsorbed layers, the mass will no longer couple completely to the oscillatory motion of the crystal. Thus if modeled via Sauerbrey when actually a more complex viscoelastic model should be used, then the mass will be underestimated.

QCM-D uses multiple overtones to model viscoelastic properties and also to determine an accurate thickness for films that disobey the Sauerbrey relation. The most commonly used viscoelastic model is the Voigt model [34]. The Voigt model is associated with soft films (high ΔD) – especially if the harmonic responses don't overlap for all the overtones. This model considers the film to have both viscous and elastic properties, which are illustrated in Figure 20a by a spring and dashpot in a parallel circuit diagram. An accompanying double y-axis plot in Figure 20b depicts the deformation and force versus time for these same parallel circuits. It is important to note the extent to which deformation lags behind the applied force – a clear example of energy being dissipated.

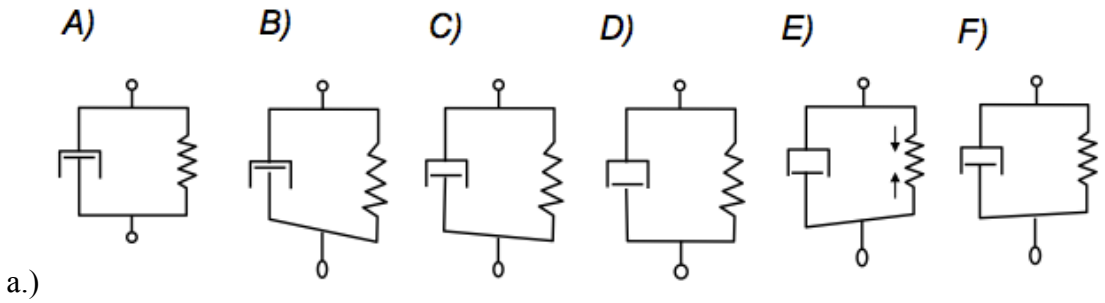

a.)

Figure 20. Voigt model representations. Parts a) and b) depict circuit and graphical representations respectively of the Voigt model system undergoing deformation. Used with permission from Biolin Scientific.

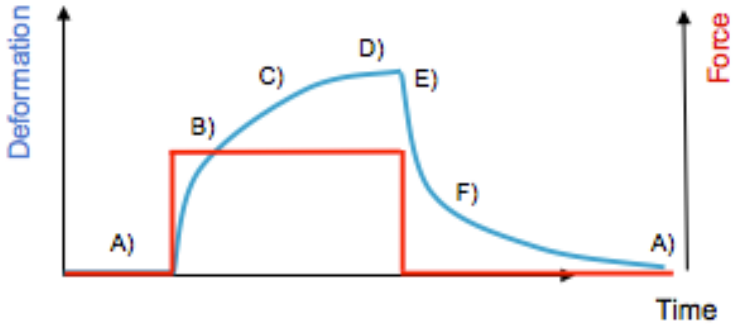

b.)

Figure 20. Continued.

Proper application of the Voigt model involves first choosing input parameters and then performing several iterations to obtain fitted Δf and ΔD values similar to the raw data. There are two variations of the Voigt model, with the main difference between the two being that one has a frequency dependence (extended Voigt model) and the other does not (standard Voigt model). A simple way to visualize this frequency dependence is to consider how Silly Putty responds to defomation. For example, if the Silly Putty is allowed to sit on a surface it will eventually flow, i.e. the polymer chains gradually disentangle. On the other hand, if the Silly Putty is rapidly stretched then fracture occurs.

The standard Voigt model involves the input of frequency and dissipation changes from multiple overtones (at least two required), layer density, bulk fluid density, and bulk fluid viscosity. The resulting outputs are film thickness, viscosity, and storage modulus. These outputs are components of the following equation:

$$\mu^* = \mu' + j2\pi f\eta \qquad 94.3)$$

where μ' = storage modulus and η = viscosity [61]. This model assumes that the film is laterally homogenous, that the bulk fluid is Newtonian, that the adsorbed layer is rigidly attached to the crystal, and that the film itself is viscoelastic. Figure 21 illustrates the overtone responses as they propagate through the crystal, film, and then bulk liquid [61].

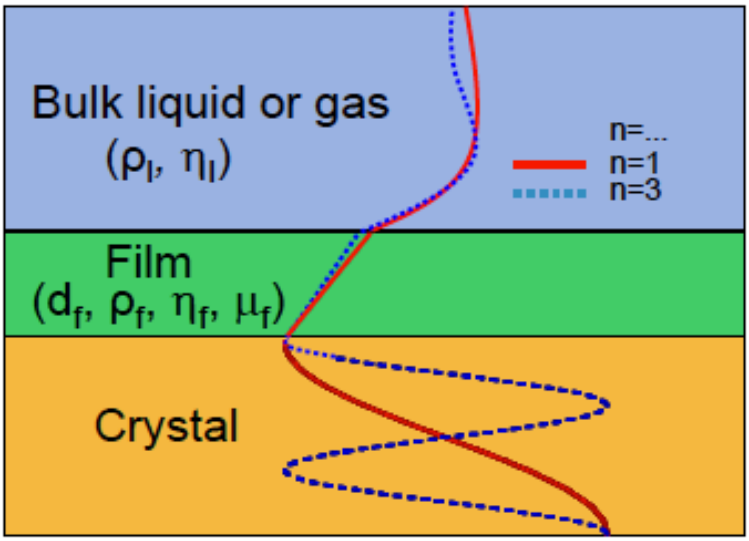

Figure 21. A depiction of overtone propagation throughout the various mediums encountered during a typical QCM-D experiment. These responses are quite complex, thus in order to determine film properties accurately the Voigt model is applied. Used with permission from Biolin Scientific.

The procedure for the extended Voigt model is essentially the same as for the standard Voigt model, with the main exceptions being the addition of frequency dependent parameters for both viscosity and storage modulus. The actual viscosity and storage modulus values are thus determined via the following two equations:

$$\eta_n = \eta_0 \left(\frac{f_n}{f_0} \right)^{\alpha^\eta} \tag{4.4}$$

$$G_n^{'} = G_0^{'} \left(\frac{f_n}{f_0} \right)^{\alpha'} \tag{4.5}$$

where α^η = frequency dependent viscosity parameter and α' = frequency dependent shear parameter [61]. Typically during the modeling process the parameters α^η and α' are set to vary from -2 to 0 and 0 to 2 respectively. Table 4 shown below includes some example values from literature that were found via the Voigt modeling routine.

Table 4. Example Values Found via Application of the Voigt Model.

Material	*Viscosity (kg $m^{-1}s^{-1}$)*	*Shear Modulus (Pa)*	*Density (kg m^{-3})*
Human Fibrinogen [62]	0.0010-0.0045	N.A.	1200
Estrogen Response Element [63]	2E-3	1.9E5	1069 (84% H_2O)
Mytilys edilus foot protein [64]	Prior to crosslinking: 1.8E-3 After crosslinking: 6E-3	Prior to crosslinking: 6.6E4 After crosslinking: 30E4	Prior to crosslinking: 1040 After crosslinking: 1180

When obtaining such values with QCM-D it must be realized that this technique measures water coupled as an inherent mass via direct hydration, viscous drag, and/or entrapment in cavities in the adsorbed film [61]. Thus an additional technique should be utilized in order to obtain the actual film mass as opposed to the hydrated mass.

4.4 TROUBLESHOOTING

Due to the fact that QCM-D is such a sensitive technique, great care must be taken in order to obtain the best possible data. As a general rule, whenever a problem arises it is best to consult with either the QCM-D user manual, the Q-Sense website, or the designated Q-Sense representative. What follows is a general overview of the most common issues encountered herein over the course of this thesis work along with possible resolutions.

The predominant problem encountered in this thesis work was traceable to the crystal condition. According to Q-Sense, under ideal conditions the crystal can be reused 10-30 times [61]. In practice, this has rarely been the case. A single crystal can really be used 5-10 times, but the crystal quality understandably degrades a little after each use. Some obvious signs that a crystal should be discarded include cracks along the edges or scratches and holes in the sensor coating. Further evidence indicating a crystal has passed its usable life is that the measurement signal becomes noisy and shaky. In fact it sometimes becomes difficult to even obtain a stable baseline for the 3rd overtone.

So what can be considered an acceptable crystal measurement? According to Q-Sense, the baseline for frequency and dissipation should be stable (e.g. a clean non-coated standard gold crystal in water should not drift more than 2 Hz/hour and 0.2x10-6 dissipation units) [61]. For possible causes for frequency and dissipation drifts the reader is directed to the FAQ section on the Q-Sense website. Additional parameters to consider are that the noise levels should be lower than 0.6 Hz (peak-to-peak) and

0.15x10-6 (peak-to-peak) respectively when measured within a period of 2 minutes [61]. One last indicator that the crystal can be considered suitable for use is that the absolute frequency value of the fundamental resonance should be in the interval 4,900-5,000 kHz [61].

The next most common set of issues encountered during this thesis work were connected to the actual assembly process. Theoretically whenever assembly of an LbL film is initiated using QCM-D, one would expect to see a decrease in Δf and a corresponding increase in ΔD. In some cases this does not occur. Q-Sense states that this potentially is caused by a number of factors, some of which include faulty crystal cleaning prior to experiment start (i.e. species are desorbing from crystal), different bulk fluids being used throughout the experiment, or crystal "settling" during measurement (i.e. poor crystal mounting on O-ring within the cell prior to experiment start) [61].

The second problem found during the assembly process dealt with total damping or lost sensitivity of the crystal. The maximum allowed thickness of a film depends on its viscoelasticity, and may vary from a couple hundred nanometers to a few microns. Thus, the more rigid the layer then the larger the possible thickness can be. In order to avoid overloading the crystal it is good practice to reduce the concentration of the assembly solutions. This is a tricky balance however, because if the concentration is too high then one may experience bulk effects or too rapid kinetics, but if the concentration is too low then a response may not even be observed.

The third and final assembly-related issue concerned bubbles in the tubing. On some occasions bubbles still occurred despite best efforts. If these bubbles become a

major issue of concern, one potential solution that Q-Sense recommends is to degas the samples prior to use. Other solutions could include replacing O-rings and/or tubing to ensure a tight seal for the cell.

5. SUMMARY AND CONCLUSIONS

Layer-by-layer (LbL) assembly is a simple and cost-effective technique for fabrication of uniform thin films. LbL films, which can be assembled from materials such as polyelectrolytes, nanoparticles, and certain biomaterials, have proven to be effective in a host of applications ranging from optics to drug delivery. The focus of this thesis centered upon PDAC/PSS LbL assemblies containing SiO_2 and Laponite (LAP). A very pressing issue in the study of LbL films is the characterization of thermal properties, especially the glass transition temperature. A thorough understanding of these thermal properties is very important in expanding the applicability of LbL films because their properties are typically dependent on whether they are in the glassy or rubbery state.

Both MDSC and QCM-D are techniques that have recently proven quite useful in the thermal analysis of LbL systems such as PDAC/PSS and PAH/PAA. In the work presented here, layers of negatively charged nanoparticles of either spherical (SiO_2) or platelet (LAP) morphology were inserted at varying locations throughout PDAC/PSS LbL films. QCM-D and MDSC were then used to determine the effect that these nanoparticles have on the previously measured thermal transitions as a function of placement within the film and particle shape. Using QCM-D we have observed clear, reproducible T_g's in all LAP film configurations and in one particular SiO_2 configuration. All observed T_g's, regardless of nanoparticle morphology, were elevated with respect to those found in neat PDAC/PSS films. In addition, there was little

difference noted between the transition values for the two particular morphologies. It was discovered that the highest glass transition temperatures were observed for film configurations where the nanoparticles were added during the middle bilayer. We attributed this phenomenon to the increased available nanoparticle surface area with which nearby polymer chains could form bonds. Unfortunately the extremely weak and broad thermal transitions observed with MDSC proved to be inconclusive in either supporting or refuting these observations made via QCM-D. Future work will focus on thermal analysis of PDAC/PSS complexes using QCM-D.

REFERENCES

[1] Decher, G. *Science.* **1997,** *277,* 1232.

[2] Iler, R. K. J. *Colloid Interface Sci.* **1966,** *21,* 569.

[3] Laschewsky, A.; Mayer, B.; Wischerhoff, E.; Arys, X.; Bertrand, P.; Delcorte, A.; Jonas, A. *Thin Solid Films.* **1996,** *284-285,* 334.

[4] Langer, R. *Nature.* **1998,** *392,* 5.

[5] Peyratout, C. S.; Dähne, L. *Angew. Chem., Int. Ed.* **2004,** *43,* 3762.

[6] Constantine, C. A.;Mello, S. V.; Dupont, A.; Cao, X.; Santos, D.; Oliveira, O. N.; Strixino, F. T.; Pereira, E. C.; Cheng, T.-C.; Defrank, J. J.; et al. *J. Am. Chem. Soc.* **2003,** *125,* 1805.

[7] Decher, G.; Lehr, B.; Lowack, K.; Lvov, Y.; Schmitt, *J. Biosens. Bioelectron.* **1994,** *9,* 677.

[8] Cheung, J. H.; Fou, A. F.; Rubner, M. F. *Thin Solid Films.* **1994,** *244,* 985.

[9] Guzman, E.; Ritacco, H.; Rubio, J. E. F.; Rubio, R. G.; Ortega, F. *Soft Matter.* **2009,** *5,* 2130.

[10] Liu, G.; Zou, S.; Fu, L.; Zhang, G. *J. Phys. Chem. B.* **2008,** *112,* 4167.

[11] Wong, J. E.; Zastrow, H.; Jaeger, W.; von Klitzing, R. *Langmuir.* **2009,** *25,* 14061.

[12] Schlenoff, J. B.; Dubas, S. T. *Macromolecules.* **2001,** *34,* 592.

[13] Steitz, R.; Leiner, V.; Siebrecht, R.; von Klitzing, R. *Colloids Surf. A.* **2000,** *163,* 63.

[14] Choi, J.; Rubner, M. F. *Macromolecules.* **2005,** *38,* 116.

[15] Shiratori, S. S.; Rubner, M. F. *Macromolecules.* **2000,** *33,* 4213.

[16] Lvov, Y.;Antipov, A. A.;Mamedov,A.;Möhwald, H.; Sukhorukov, G. B. *Nano Lett.* **2001,** *1*, 125.

[17] Büscher, K.; Graf, K.; Ahrens, H.; Helm, C. A. *Langmuir*. **2002,** *18,* 3585.

[18] Tan, H. L.; McMurdo, M. J.; Pan, G.; Van Patten, P. G. *Langmuir.* **2003,** *19,* 9311.

[19] Gopinadhan, M.; Ahrens, H.; Günther, J.-U.; Steitz, R.; Helm, C. A. *Macromolecules.* **2005,** *38,* 5228.

[20] Secrist, K. E.; Nolte, A. J. *Macromolecules.* **2011,** *44,* 2859.

[21] Schlenoff, J. B.; Dubas, S. T.; Farhat, T. *Langmuir.* **2000,** *16,* 9968.

[22] Nogueira, G. M.; Banerjee, D.; Cohen, R. E.; Rubner, M. F. *Langmuir.* **2011,** *27,* 7860.

[23] Bieker, P.; Schonhoff, M. *Macromolecules.* **2010,** *43,* 5052.

[24] Picart, C.; Mutterer, J.; Richert, L.; Luo, Y.; Prestwich, G. D.; Schaaf, P.; Voegel, J.-C.; Lavalle, P. Proc. Natl. Acad. Sci. U. S. A. **2002,** *99,* 12531.

[25] Schmitt, J.; Gruenewald, T.; Decher, G.; Pershan, P. S.; Kjaer, K.; Loesche, M. *Macromolecules.* **1993,** *26,* 7058.

[26] Köhler, K.; Möhwald, H.; Sukhorukov, G. B. *J. Phys. Chem. B.* **2006,** *110,* 24002.

[27] Mueller, R.; Köhler, K.; Weinkamer, R.; Sukhorukov, G.; Fery, *Macromolecules.* **2005,** *38,* 9766.

[28] Nazaran, P.; Bosio, V.; Jaeger, W.; Anghel, D. F.; von Klitzing, R. *J. Phys. Chem. B.* **2007,** *111,* 8572.

[29] Ghostine, R. A.; Schlenoff, J. B. *Langmuir.* **2011,** *27,* 8241.

[30] Shao, L.; Lutkenhaus, J. L. *Soft Matter.* **2010,** *6,* 3363.

[31] Tammelin, T.; Merta, J.; Johansson, L.-S.; Stenius, P. *Langmuir.* **2004,** *20,* 10900.

[32] Dixon, M. C. *J. Biomol. Tech.* **2008,** *19,* 151.

[33] Sauerbrey, G. Z. *Physics.* **1959,** *155,* 206.

[34] Voinova, M. V.; Rodahl, M.; Jonson, M.; Kasemo, B. Phys. Scr. **1999,** *59,* 391.

[35] L. C. Thomas, Modulated DSC® Technology, **2006.**

[36] Lavalle, P.; Picart, C.; Mutterer, J.; Gergely, C.; Reiss, H.; Voegel, J. C.; Senger, B.; Schaaf, P. *J. Phys. Chem. B.* **2004,** *108,* 635.

[37] Vidyasagar, A.; Sung, C.; Gamble, R.; Lutkenhaus, J. L. *ACS Nano.* **2012,** *6,* 6174.

[38] Vidyasagar, A.; Sung, C.; Losensky, K.; Lutkenhaus, J. L. *Macromolecules*. **2012,** *45,* 9169**.**

[39] Ishida, N.; Biggs, S. *Langmuir.* **2007,** *23,* 11083.

[40] Martin, S. J.; Granstaff, V. E.; Frye, G. C. *Anal. Chem.* **1991,** *63,* 2272.

[41] Zhu, D. M.; Fang, J. J.; Wu, B.; Du, X. B. *Phys. Rev. E.* **2008,** *77.*

[42] Köhler, K.; Biesheuvel, P. M.; Weinkamer, R.; Möhwald, H.; Sukhorukov, G. B. *Phys. Rev. Lett.* **2006,** *97.*

[43] Köhler, K.; Shchukin, D. G.; Möhwald, H.; Sukhorukov, G. B. *J. Phys. Chem. B.* **2005,** *109,* 18250**.**

[44] Gauczinski, J.; Liu, Z.; Zhang, X.; Schonhoff, M. *Langmuir.* **2010,** *26,* 10122.

[45] Fortier-McGill, B.; Reven, L. *Macromolecules.* **2008,** *42,* 247.

[46] Lvov, Y.; Ariga K.; Onda, M.; Izumi, I; Kunitake, T. *Langmuir.* **1997,** *13,* 6195.

[47] Kleinfeld, E. R.; Ferguson, G. S. *Science.* **1994,** *265,* 370.

[48] Tsagaropoulos, G.; Eisenbery, A. *Macromolecules.* **1995,** *28,* 6067.

[49] Xu, D.; Hodges, C.; Ding, Y.; Biggs, S.; Brooker, A.; York, D. *Langmuir.* **2010,** *26,* 18105.

[50] Zhang, L.; Feng, G.; Zeravcic, Z.; Brugarolas, T.; Liu, A. J.; Lee, D. *ACS Nano.* **2013,** *7,* 8043.

[51] Warner, W. W.; Stockbridge, C. D. In *Vacuum Microbalance Techniques;* Walker, R. F., Ed.; Plenum, New York, Vol. 3 (1963) 55.

[52] Nomura, T.; Hattori, O. *Analytical Chimica Acta.* **1980,** *115,* 323.

[53] Kanazama, B. K.; Gordon III, J. G. *Analytica Chimica Acta.* **1985,** *175,* 99.

[54] Hook, F. Protein Adsorption with a Newly Developed Quartz Crystal Microbalance. PhD. Dissertation, Chalmers University of Technology, Sweden, 1997.

[55] Rodal, M. On the Frequency and Q Factor Response of the Quartz Crystal Microbalance to Liquid Overlayers. PhD. Dissertation, Chalmers University of Technology, Sweden, 1995.

[56] Cady, W. G. *Piezoelectricity,* 2nd ed.; Dover: New York, (1964).

[57] Salt, D. *Hy-Q handbook of Quartz Crystal Devices;* Van Nostrand Reinhold (UK) Co. Ltd: Padstow, Cornwall, (1987).

[58] Lack, F. R.; Wilard, G. W.; Fair, I. E. *Bell System Technical Journal.* **1934,** *13,* 453.

[59] Buttry, D.; Ward, M. *Chem. Rev.* **1992,** *92,* 1355.

[60] Sauerbrey, G. *Arch. Elektr. Ubertrag*. **1964,** *18,* 617.

[61] Q-Sense QCM-D Training Publications.

[62] Weber, N.; Pesnell, A.; Bolikal, D.; Zeltinger, J.; Kohn, J. *Langmuir.* **2007,** *23,* 3298.

[63] Peh, W. Y.; Reimhult, E.; Teh, H. F.; Thomsen, J. S.; Su, X. *Biophys. J.* **2007,** *92,* 4415.

[64] Hook, F.; Kasemo, B. *Anal. Chem.* **2001,** *73,* 5796.